Development of a Conceptual Process for Selective CO_2 Capture from Fuel Gas Streams Using [hmim][Tf2N] Ionic Liquid as a Physical Solvent

Omar M. Basha[1,2], Murphy J. Keller[1], David R. Luebke[1], Kevin P. Resnik[1,3] and Badie I. Morsi[1,2]

[1] *U.S. Department of Energy, National Energy Technology Laboratory*
P.O. Box 10940, Pittsburgh, PA 15236

[2] *Department of Chemical and Petroleum Engineering*
University of Pittsburgh, Pittsburgh, PA 15261

[3]*URS Corporation, Pittsburgh, PA 15236*

1. ABSTRACT

The Ionic Liquid (IL) [hmim][Tf2N] was used as a physical solvent in an Aspen Plus simulation, employing the Peng-Robinson Equation of State (P-R EOS) with Boston-Mathias (BM) alpha function and standard mixing rules, to develop a conceptual process for CO_2 capture from a shifted warm fuel gas stream produced from Pittsburgh # 8 coal for a 400 MWe power plant. The physical properties of the IL, including density, viscosity, surface tension, vapor pressure and heat capacity were obtained from literature and modeled as a function of temperature. Also, available experimental solubility values for CO_2, H_2, H_2S, CO, and CH_4 in this IL were compiled and their binary interaction parameters (δ_{ij} and l_{ij}) were optimized and correlated as functions of temperature. The Span-Wager Equation-of-State EOS [1] was also employed to generate CO_2 solubilities in [hmim][Tf2N] at high pressures (up to 10 MPa) and temperatures (up to 510 K).

The conceptual process developed consisted of 4 adiabatic absorbers (2.4 m ID, 30 m high) arranged in parallel and packed with Plastic Pall Rings of 0.025 m for CO_2 capture; 3 flash drums arranged in series for solvent (IL) regeneration with the pressure-swing option; and a pressure-intercooling system for separating and pumping CO_2 up to 153 bar to the sequestration sites. The compositions of all process streams, CO_2 capture efficiency, and net power were calculated using Aspen Plus simulator. The results showed that, based on the composition of the inlet gas stream to the absorbers, 95.67 mol% of CO_2 was captured and sent to sequestration sites; 99.5 mol% of H_2 was separated and sent to turbines; the solvent exhibited a minimum loss of 0.31 mol%; and the net power balance of the entire system was 30.81 MW. These results indicated that [hmim][Tf2N] IL could be used as a physical solvent for CO_2 capture from warm shifted fuel gas streams with high efficiency.

2. INTRODUCTION AND BACKGROUND

The Ionic Liquid [hmim][Tf_2N], known as 1-hexyl-3-methylimidazolium bis(trifluoro-methylsulfonyl)amide, or 1-hexyl-3-methylimidazoliumbis(trifluoromethylsulfonyl)imide (structure is shown in Figure 1) was selected by the International Union of Pure and Applied Chemistry (IUPAC) as a reference fluid in order to establish a reliable data bank for its thermodynamic as well as thermo-physical properties and to measure high pressure solubilities of different gases, such as CO_2, CO, H_2, CH_4, H_2O, Xe, etc. in this IL. The selection of [hmim][Tf_2N] was made because of its stability, low viscosity, low water solubility, and ease of preparation as well as purification [2], [3]. This paper is focusing on the application of this IL as a physical solvent for CO_2 capture from warm fuel gas streams.

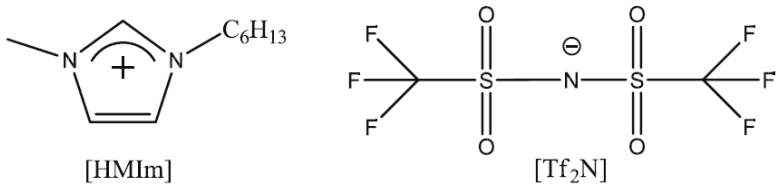

Figure 1: Molecular Structure of the Ionic Liquid [hmim][Tf2N]

Shiflett et Yokozeki [4] measured the solubility of CO_2 in an ultrapure sample from NIST (IUPAC task force sample) and in a commercially available sample of [hmim][Tf2N] using a gravimetric microbalance at different temperatures (282, 297, 323, and 348 K) and under pressures up to about 2 MPa. Their experimental P-T-X data were correlated with an Equation-of-state and the predicted CO_2 solubility values in VLL were comparable with those available in the literature. Kumełan et al. [5] presented experimental solubility data for H_2 in [hmim][Tf_2N] at 293 to 413 K under pressures up to about 10 MPa. The solubility of H_2 in this IL was found to be low and the values increased with temperatures. They extended Henry's law to correlate the solubility pressures. These authors also reported a H_2 solubility of 0.170 mol of H_2/kg of IL at T = 413 K and pressure ≈ 9 MPa. Anderson et al. [6] measured the solubility of sulfur dioxide SO_2 in ([hmim][Tf2N] and in another IL 1-n-hexyl-3-methylpyridinium bis(trifluoromethylsulfonyl)imide, [hmpy][Tf2N] at temperatures from 485 and 520 K and pressures up to 0.4 MPa. Their data indicated that large amounts of SO_2 (up to 85 mol %) were physically absorbed in the ILs.

Kumełan et al. [7] reported experimental results for the solubility of CH_4 and Xe in [hmim][Tf_2N] at temperatures from 293.3 to 413.3 K, and the maximum pressure of 9.6 MPa where the solubilities for both gases decreased with temperature. The maximum solubility of CH_4 was 0.51 mol·kg^{-1} at 9.3 MPa and that of Xe at 9.6 MPa was 2.08 mol·kg^{-1}. They mentioned that Xe showed significantly greater solubility than CH_4 under all conditions investigated. The Henry's constants (at zero pressure) for CH_4 and Xe in the IL were also correlated as a function of temperature. Kumełan et al. [8] measured CO and O_2 solubilities in [hmim][Tf_2N] at temperatures from 293.25 to 413.2 K under pressures up to 9.8 MPa using a high-pressure view-cell technique. They reported that the solubilities decreased with increasing temperature and O_2 had a slightly higher solubility than that of CO under all conditions investigated, however, the solubility values generally remained very low. The maximum CO solubility obtained at 9.8 MPa was 0.27 mol·kg^{-1} and the maximum O_2 solubility obtained at 9.1 MPa was 0.31 mol·kg^{-1}. Also, an extension of Henry's law was employed to correlate the CO and O_2 solubilities in the IL.

Raeissi et al. [9] measured the solubility of H_2 in [hmim][Tf2N] at various temperatures up to 370 K and pressures up to 12 MPa. Their results showed good agreement with those of two other laboratories focusing on measuring H_2 solubilities in the same IUPAC sample using different experimental setups. Florusse et al. [10] investigated the high-pressure phase behavior of the CO and [hmim][Tf2N] system within a temperature range from 300 to 440 K and under pressures up to about 12 MPa. Their results were in good agreement with those by Kumełan et al. [8].

Anderson et al. [11] showed that CO_2 has greater solubility than other gases (C_2H_4, C_2H_6, CH_4, O_2, N_2) in 1-hexyl-3-methylpyridinium bis(trifluoromethylsulfonyl)imide [hmpy][Tf_2N] [12], and suggested that ILs could selectively capture CO_2 form flue gas streams. Furthermore, Anderson et al. [11] and Muldoon et al. [13] showed that the CO_2 solubility in ILs is strongly dependent on the composition of the anion. In addition, the mutual solubilities of water and [hmim][Tf2N]] were reported by Freire et al. [14].

Shi and Maginn [15] calculated the solubility of H_2O and CO_2 in [hmim][Tf2N]) using atomistic Monte Carlo simulations. They reported that quantitatively the computed isotherms, Henry's Law constants and partial molar enthalpies of absorption for H_2O and CO_2 in the IL were in agreement with available experimental data. The simulations also predicted that the excess molar volume of CO_2/IL was greater than that H_2O/IL and both were negative. Shi et al. [16] used classical molecular dynamics and Monte Carlo simulations to calculate the solubility of pure and mixed CO_2, H_2, and Ar gases in [hmim][Tf2N]. Their computed absorption isotherms, Henry's law constants, and partial molar enthalpies for pure H_2 agreed well with their experimental data and those obtained by Kumełan et al. [7], however, the agreement with the experimental data by Finotello et al. [17] and Costa Gomes [18] at high temperatures was poor. The interaction between CO_2 and the IL was about 6 times greater than that of H_2 and the IL and 3 times greater than that of Ar and the IL, which was in agreement with a decreasing solubility from CO_2 to Ar and to H_2. Also, for CO_2 and H_2 gaseous mixture, the solubility of CO_2 over H_2 decreased from about 30 at 313 K to about 3 at 573 K.

This purpose of this study is to utilize available literature solubility data for different gases in [hmim][Tf2N] IL in Aspen Plus simulator in order to develop a conceptual process for CO_2 capture from a shifted warm fuel gas stream produced from Pittsburgh # 8 coal for a 400 MWe power plant. The composition of this shifted gas stream is shown in Table 1 [19].

Table 1: Shifted gas composition used [19]

Component	mol%
Ar	0.48
CH_4	0.24
H_2	37.50
N_2	0.33
CO	6.27
CO_2	23.87
H_2O	30.68
NH_3	0.16
H_2S	0.47
COS	0.00

3. PROPERTIES OF [HMIM][TF2N]

The density, viscosity, surface tension, vapor pressure, heat capacity and critical properties of this IL are discussed in the following.

3.1. DENSITY:

Different density values for [hmim][Tf2N] are available in the literature [3], [5], [20], [21] at various temperatures and 0.1 MPa. These values were correlated using Equation (1) as shown in Figure 2 with a correlation coefficient (R^2) = 0.9892.

$$\rho_L = 1635.8918 - 0.8892(T) \quad (1)$$

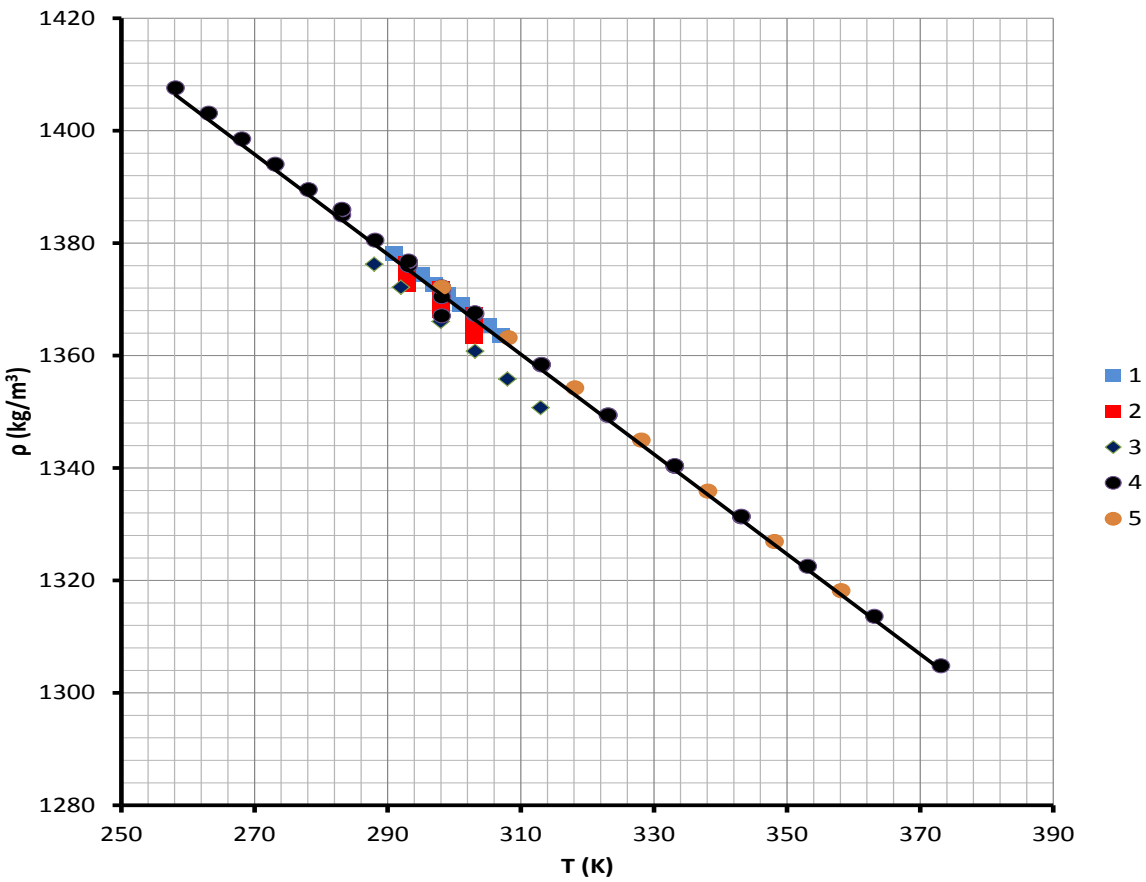

Figure 2: Density of [hmim][Tf2N] as a Function of Temperature. Compared to Experimental Data 1 [5], 2 [21], 3 [20], 4 [3] and 5 [22].

3.2. VISCOSITY:

Different viscosity values for [hmim][Tf2N] at various temperatures at 0.1 MPa were taken from the literature [3], [20], [22], [23] and correlated using Equation (2) as shown in Figure 3 with a correlation coefficient different (R^2) = 0.9987.

$$\mu_L = 0.658455e^{\left(\frac{123{,}792{,}843.733183}{T^3}\right)} \tag{2}$$

The effect of pressure on the viscosity of [hmim][Tf2N] was also accounted for (Figure 4) using similar correlation to that proposed by Muhammad et al. [22] as:

$$\frac{\mu_{L(P)}}{\mu_{L(0.1\ MPa)}} = \left(\frac{D+P}{D+0.1}\right)^E \tag{3}$$

Where:

$$D = a + bT \tag{4}$$

$$E = c + dT \tag{5}$$

With: a = 885.13, b = - 1.111, C = 22.03 and D = - 0.508

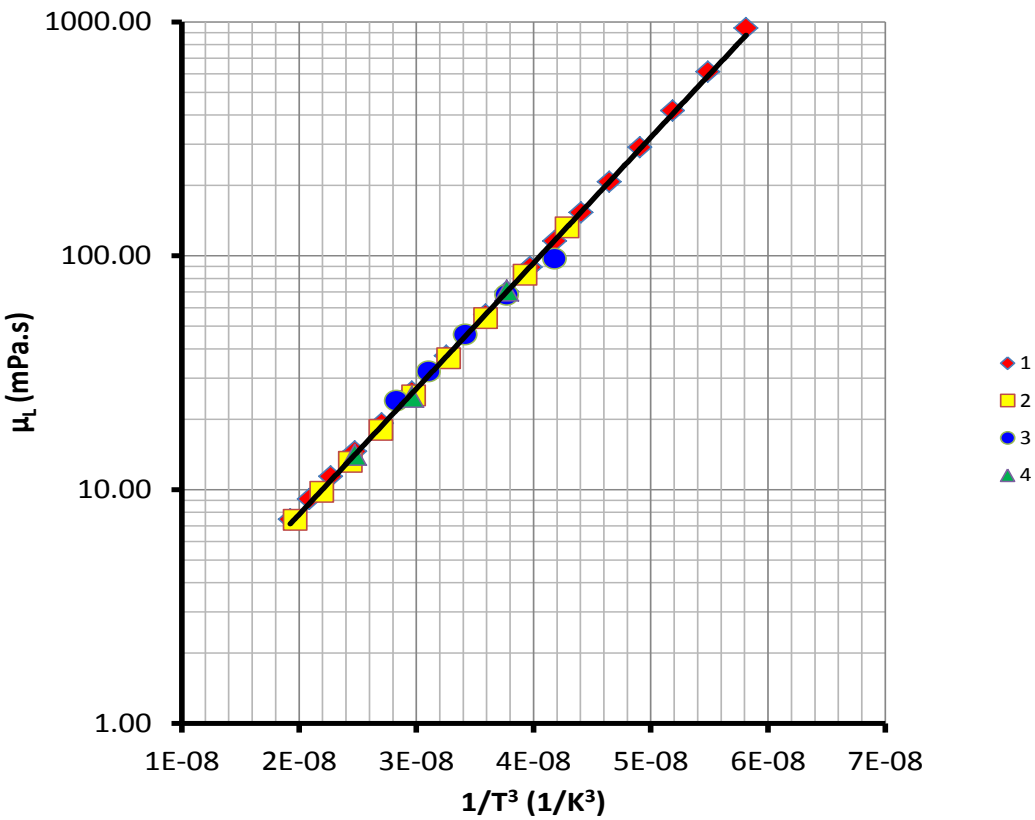

Figure 3: Viscosity of [hmim][Tf2N] as a Function of Temperature at 0.1 MPa. Compared to Experimental Data: 1[20], 2 [3], 3 [23] and 4 [22].

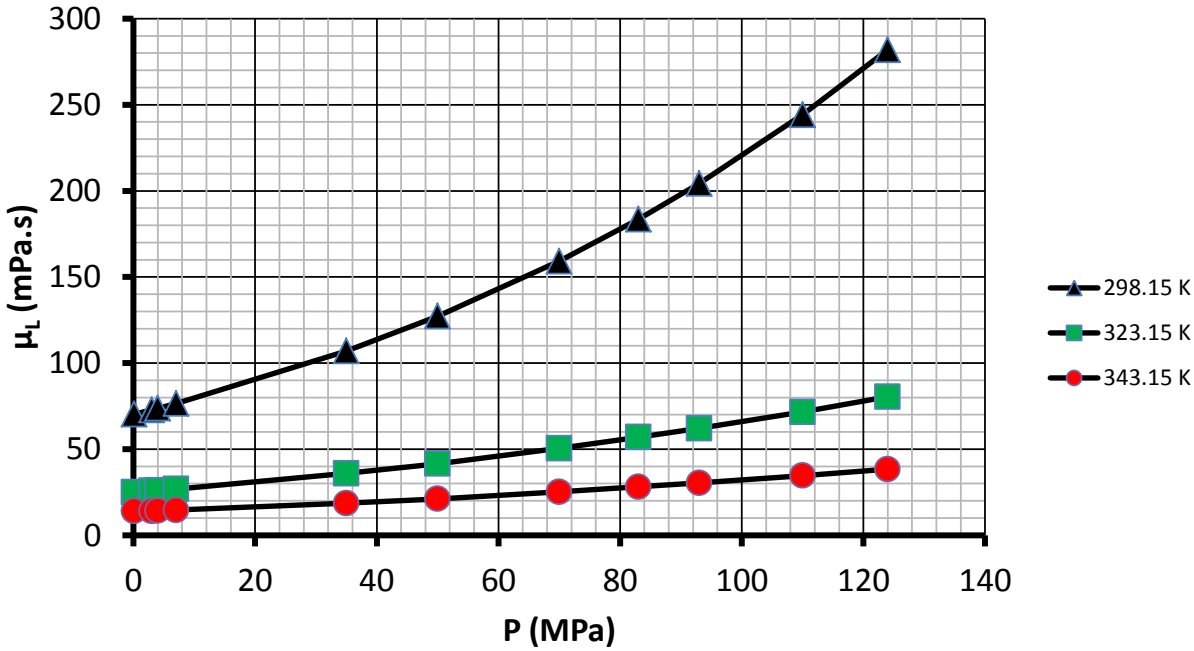

Figure 4: Effect of Pressure on the Viscosity of [hmim][Tf2N] at Different Temperatures.

3.3. SURFACE TENSION:

Various values of the surface tension of [hmim][Tf2N] were taken from the literature [5], [22], [24–27] and correlated as a function of temperature by Equation (6) as shown in Figure 5. The correlation coefficient for Equation (6) is only 0.796. It should also be mentioned that the data by Kilaru et al. [25] appear to be higher than the majority of the data and therefore their values were not taken into consideration in the development of Equation (6).

$$\sigma_L = 13.31644 - 5433.9922/T \tag{6}$$

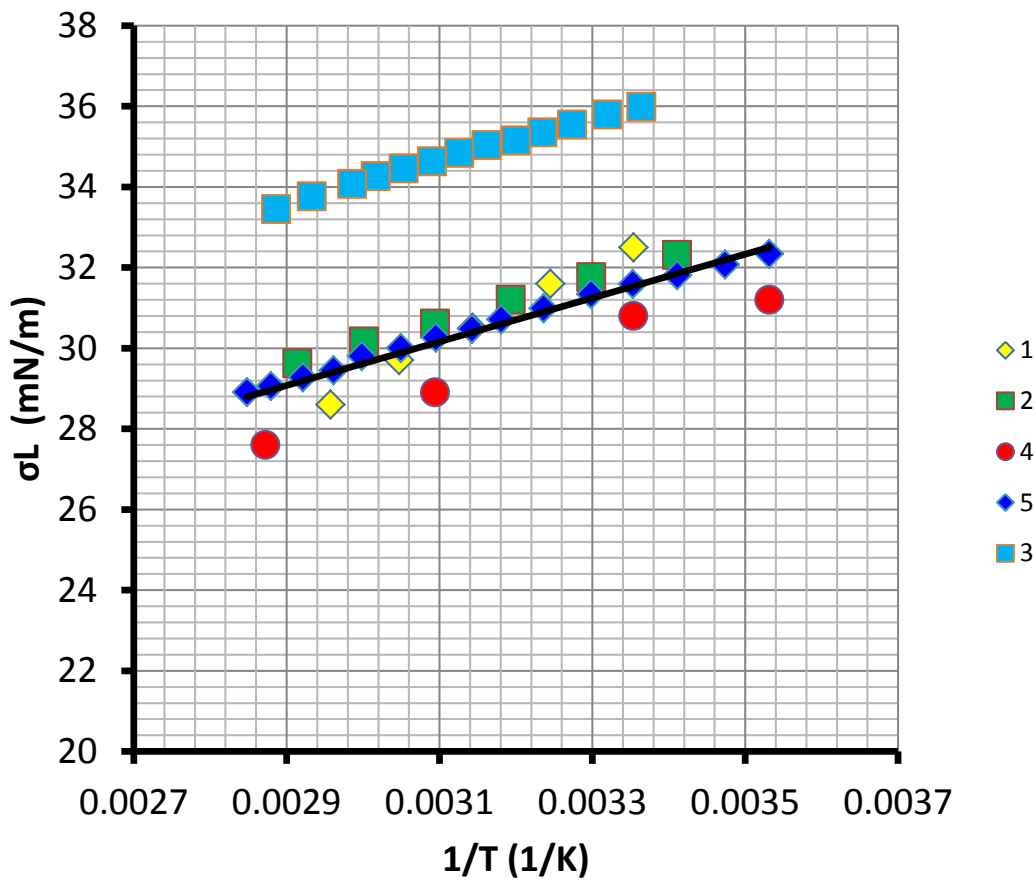

Figure 5: Surface tension of [hmim][Tf2N] as a Function of Temperature Compared to Experimental Data 1 [22], 2 [24], 3 [25], 4 [23] and 5 [27]

3.4. VAPOR PRESSURE:

The vapor pressure of [hmim][Tf2N] was reported by Zaitsau et al. [28] to be extremely low as shown in Figure 6 and the data can be correlated using Equation (7) :

$$\ln(P^{v}) = 28.31918 - 14{,}848.95148/T \tag{7}$$

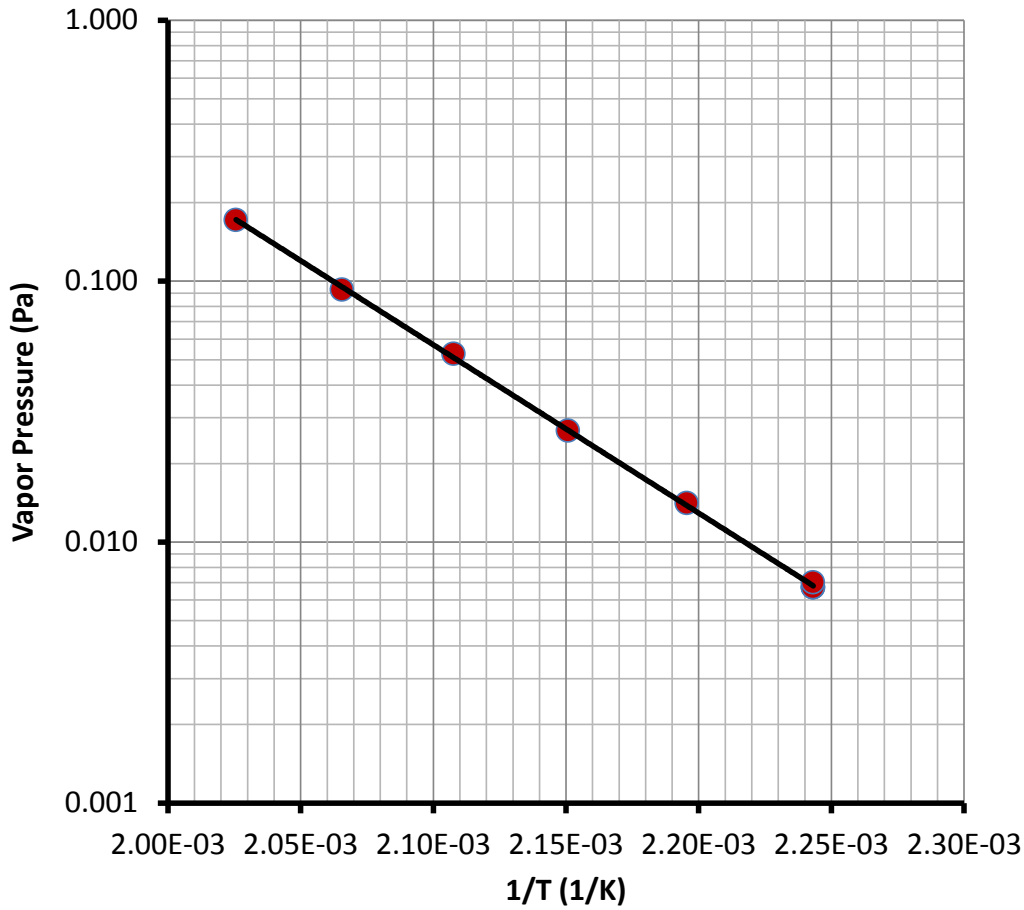

Figure 6: Vapor Pressure of [hmim][Tf2N] Compared to Experimental Data [28]

3.5. HEAT CAPACITY:

The heat capacity of [hmim][Tf2N] was reported by Shimizu et al. [29] to be relatively low as shown in Figure 7 and the data can be correlated using Equation (8) with very high correlation coefficient:

$$C_p = 0.64550 \cdot T - 439.27 \tag{8}$$

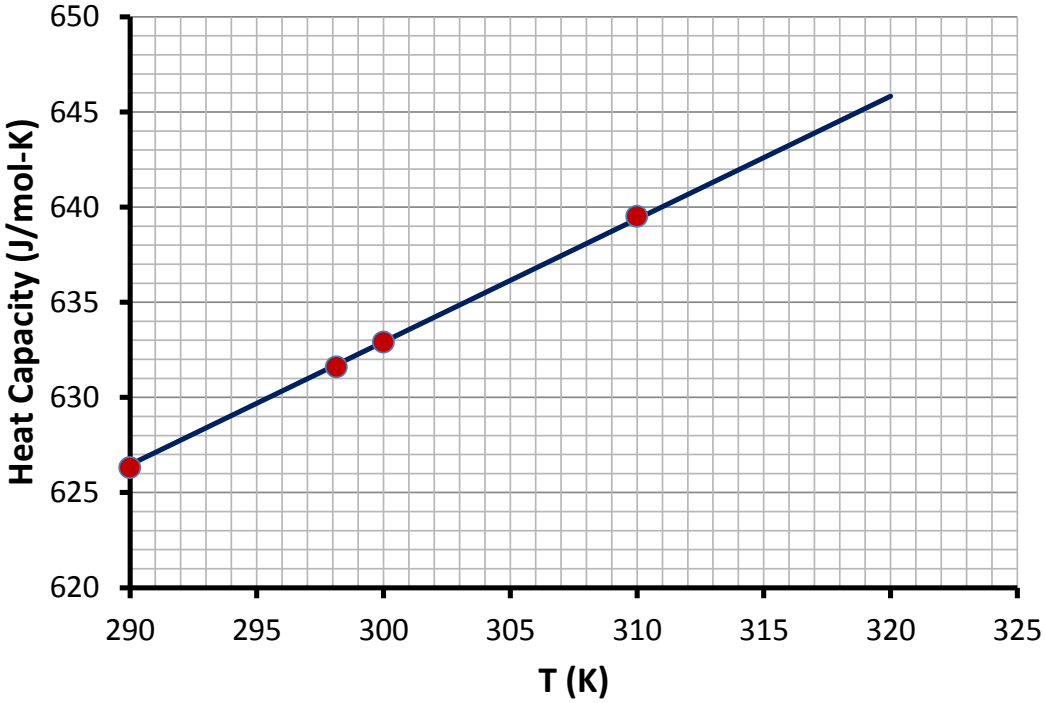

Figure 7: Heat Capacity of [hmim][Tf2N]

3.6. CRITICAL PROPERTIES:

The critical pressure (P_c) , temperature (T_c) and acentric factor for [hmim][Tf_2N] given in Table 2 were taken from Ren et al. [30]. These values were predicted using the group contributions estimation method as reported by Valderrama and Rojas [31]. The critical volume (V_c) and critical compressibility factor (Z_c) were evaluated using the correlations provided by Valderrama and Rojas [31]. These critical properties are shown in Table 2.

Table 2: [hmim][Tf_2N] critical properties

T_c, K	815	Z_c,-	0.2626
P_c, bar	16.11	ω, -	0.8556
V_c, $cm^3.mol^{-1}$	1104.4	T_b, K	714.58

4. PREDICTION OF THE BINARY INTERACTION PARAMETERS FOR THE GASES USED AND [HMIM][TF2N]

The Peng Robinson Equation of State (PR-EOS) using Boston-Mathias (BM) alpha function and standard mixing rules [32] is written as:

$$P = \frac{RT}{v_m - b} - \frac{a}{v_m(v_m + b) + b(v_m - b)} \tag{9}$$

With:

$$b = \sum_i x_i\, b_i \tag{10}$$

$$a = a_o + a_1 \tag{11}$$

In Equation (11), a_o is the standard quadratic mixing rule term, where the binary interaction parameter (δ_{ij}) is only temperature dependent.

$$a_o = \sum_i^n \sum_j^n x_i x_j\, (a_i\, a_j)^{0.5}\ (1 - \delta_{ij}) \tag{12}$$

δ_{ij} can be correlated as a function of temperature as:

$$\delta_{ij} = \delta_0 + \delta_1 T + \frac{\delta_2}{T} \qquad \text{(with } \delta_{ij} = \delta_{ji}\text{)} \tag{13}$$

On the other hand, a_1 is an additional asymptotic term used to model highly nonlinear systems.

$$a_1 = \sum_{i=1}^n x_i \left(\sum_{j=1}^n x_j [(a_i a_j)^{\frac{1}{2}}\, l_{ij}]^{1/3} \right)^3 \tag{14}$$

l_{ij} can also be correlated as a function of temperature as:

$$l_{ij} = l_0 + l_1 T + \frac{l_2}{T} \qquad \text{(with } l_{ij} = -\, l_{ji}\text{)} \tag{15}$$

Thus, $a_i = f(T, T_{ci}, P_{ci,}\omega_i)$ and $b_i = f(\, T_{ci}, P_{ci}\,)$

The coefficients δ_0, δ_1, δ_2 and l_0, l_1, l_2 in Equations (13) and (15) were optimized using the PE2000 software developed by Brunner et al. [33] and experimental solubility data and the predicted values along with the optimized binary interaction parameters for each system are illustrated for CO_2, H_2, H_2S, CH_4 and CO in Figures **8** through 17. The PE2000 tool used for the optimization employs the Simplex-Nelder-Mead algorithm for regression of the binary interaction parameters. The coefficients in Equations (13) and (15) are listed in Table 3.

Table 3: Binary interaction parameter coefficients in Equations (13) and (15)

Component	$\delta_{ij} = \delta_0 + \delta_1 \cdot T + \delta_1/T$			$l_{ij} = l_0 + l_1 \cdot T + l_1/T$		
	δ_0	δ_1	δ_2	l_0	l_1	l_2
CO_2	0.05338	-3.4649 x10^{-4}	2.3685	-0.81206	1.0058 x10^{-3}	113.665
H_2	-1.4121	1.7344 x10^{-3}	241.499	-0.4977	1.0679 x10^{-3}	106.030
CH_4	1.4941	-2.5628 x10^{-3}	-209.703	-2.0888	3.5794 x10^{-3}	326.692
CO	1.1728	-3.2704 x10^{-3}	-103.119	-1.0052	2.9159 x10^{-3}	109.641
H_2S	0.8789	-1.5492 x10^{-3}	-133.644	-0.4949	1.7573 x10^{-3}	-3.3794 x10^{-3}

Fitting and optimization results for the interaction parameters for the components CO_2, H_2, H_2S, CH_4, and CO are also shown in Figures **8** through 17.

4.1. CO_2 DATA:

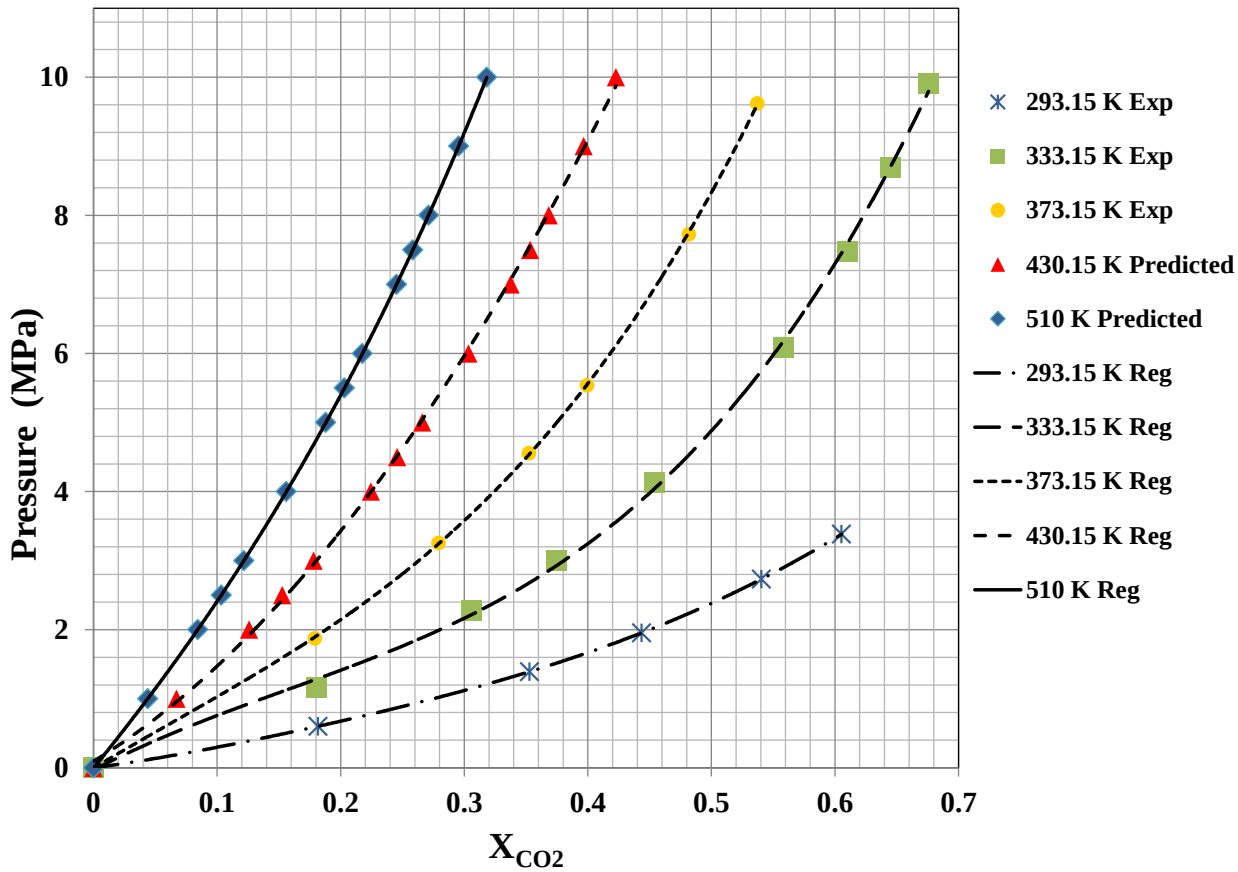

Figure 8: Comparison Between Experimental and Predicted CO_2 Mole Fractions in [hmim][Tf2N] at Different Pressures and Temperatures

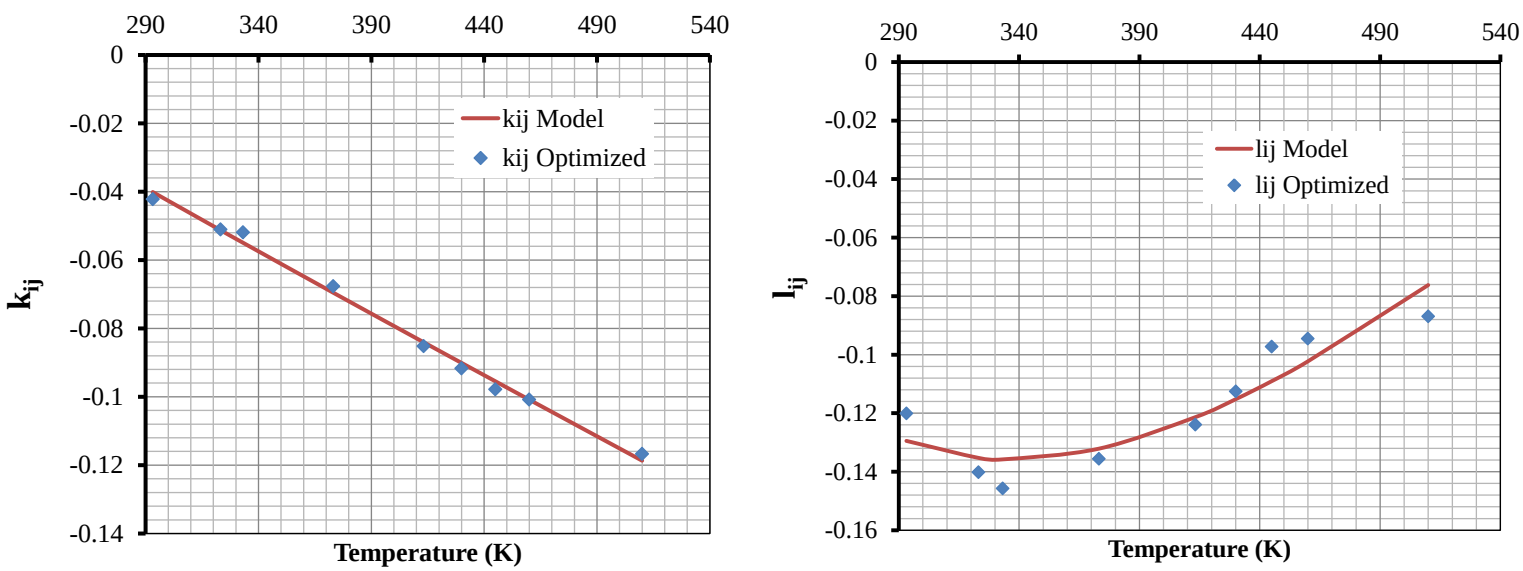

Figure 9: Optimized Binary Interaction Parameters for CO_2 in [hmim][Tf2N]

4.2. H_2 DATA:

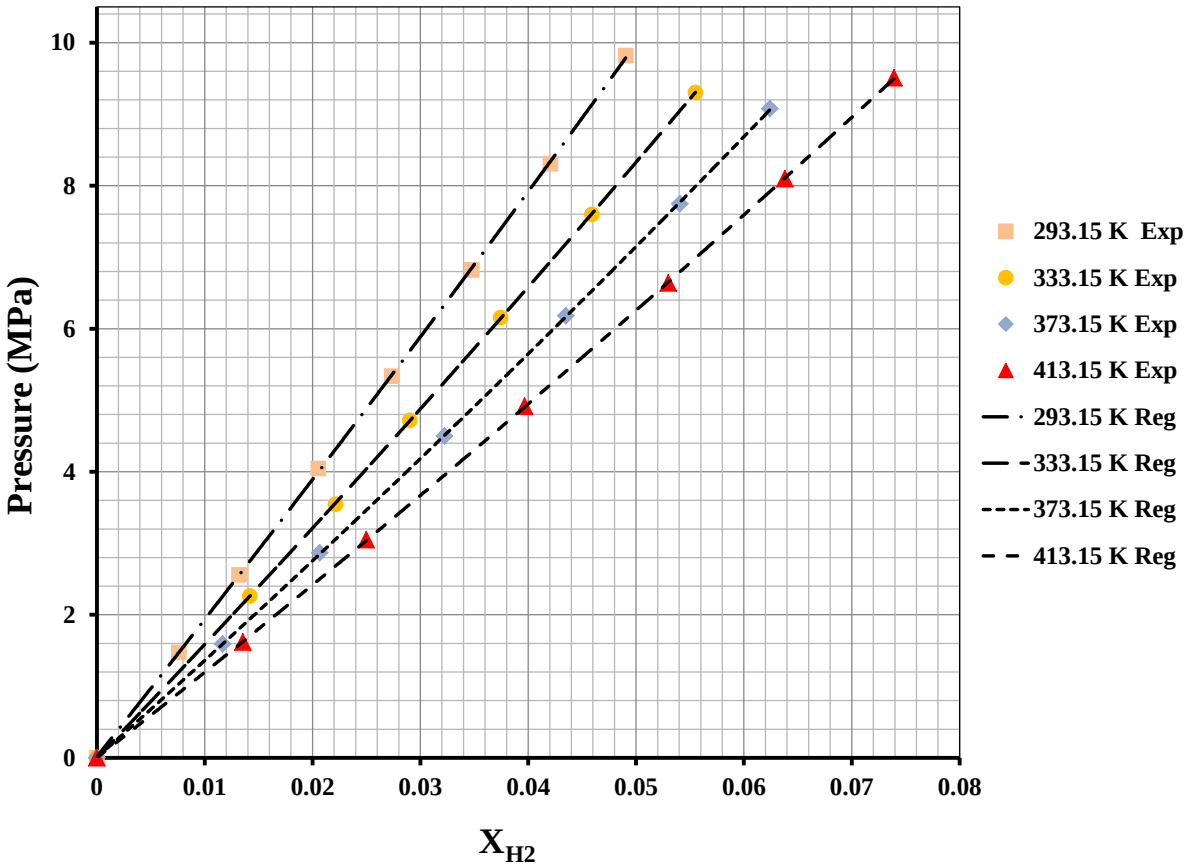

Figure 10: Comparison Between Experimental and Predicted H_2 Mole Fractions in [hmim][Tf2N] at Different Pressures and Temperatures

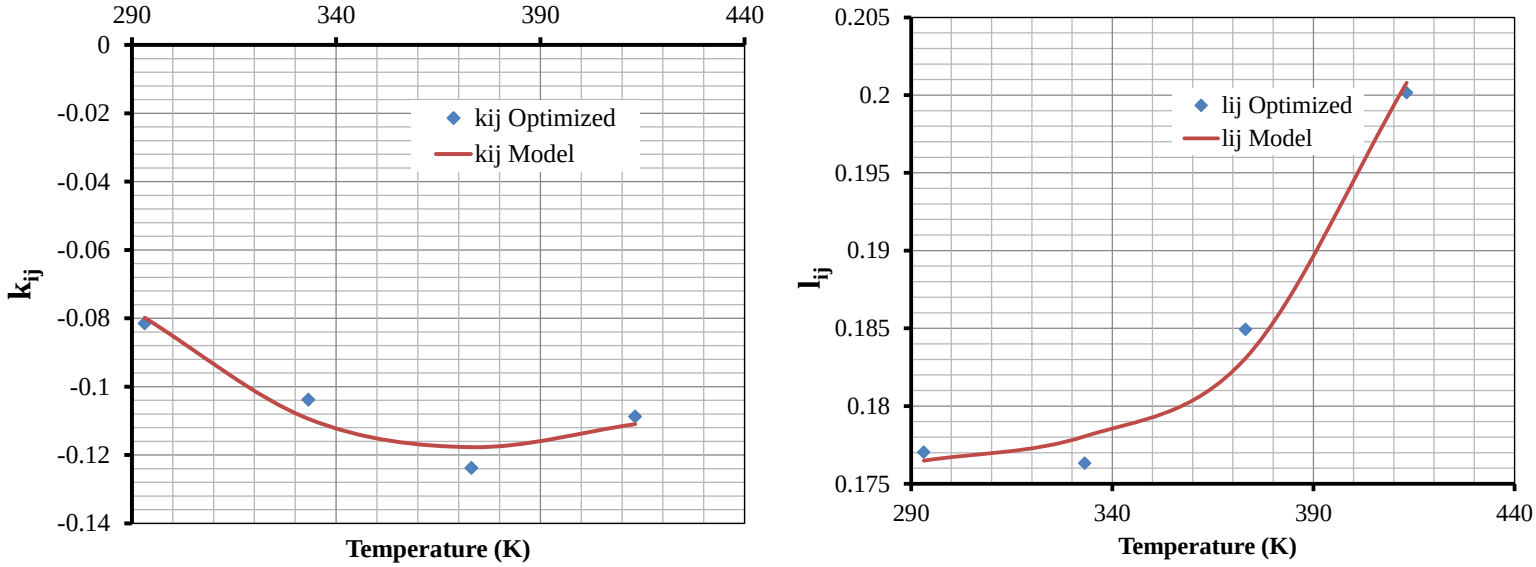

Figure 11: Optimized Binary Interaction Parameters for H_2 in [hmim][Tf2N]

4.3. H_2S DATA:

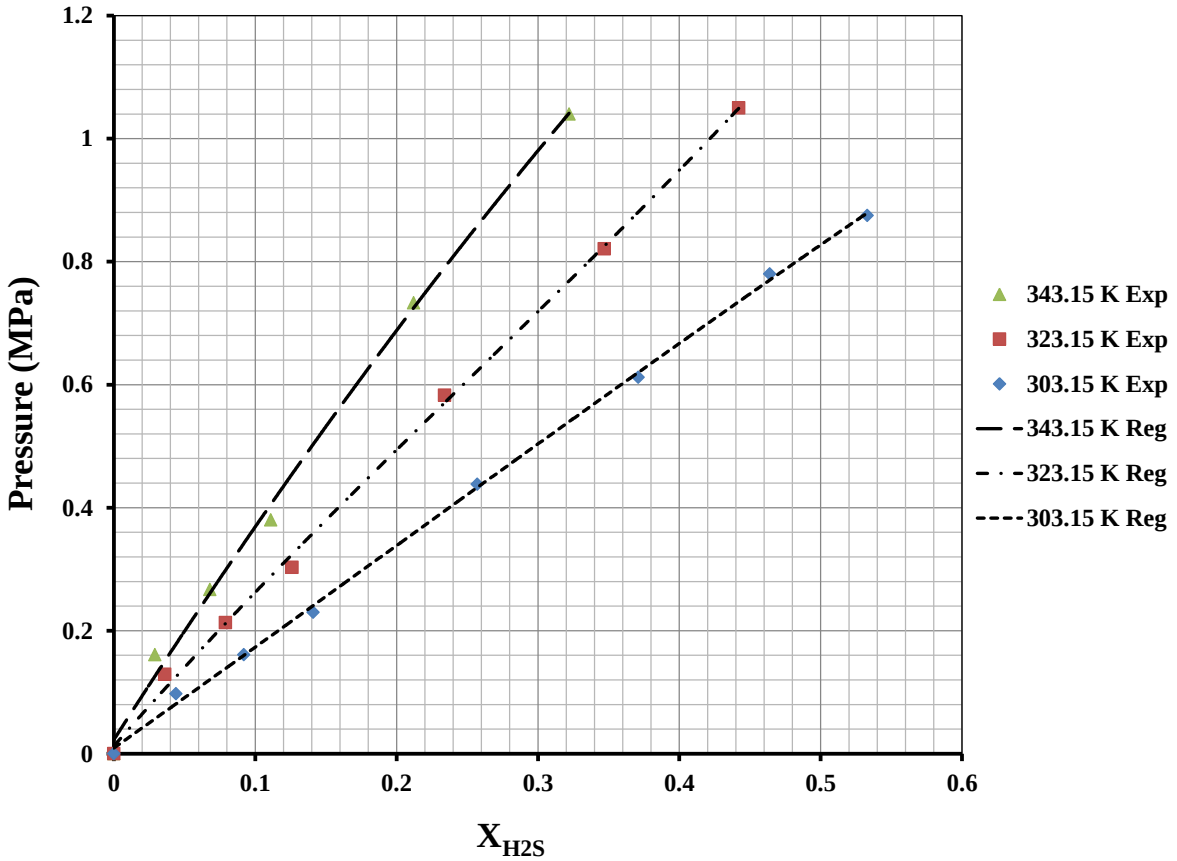

Figure 12: Comparison Between Experimental and Predicted H_2S Mole Fractions in [hmim][Tf2N] at Different Pressures and Temperatures

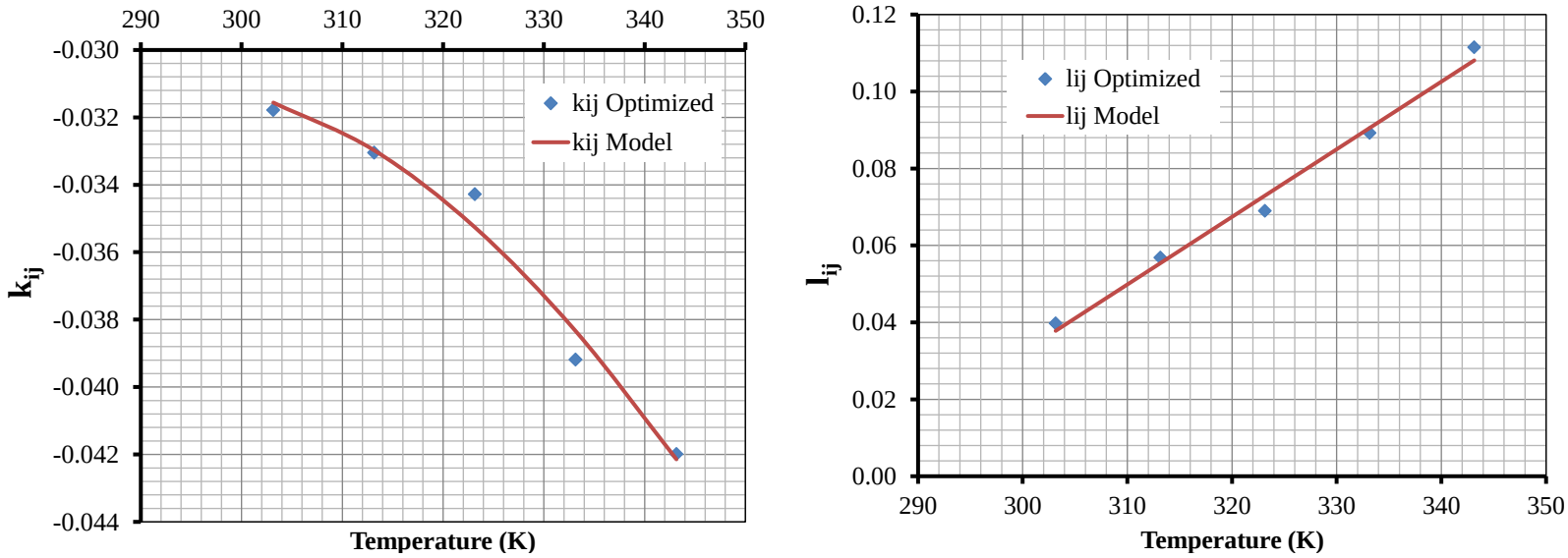

Figure 13: Optimized Binary Interaction Parameters for H_2S in [hmim][Tf2N]

4.4. CH_4 DATA:

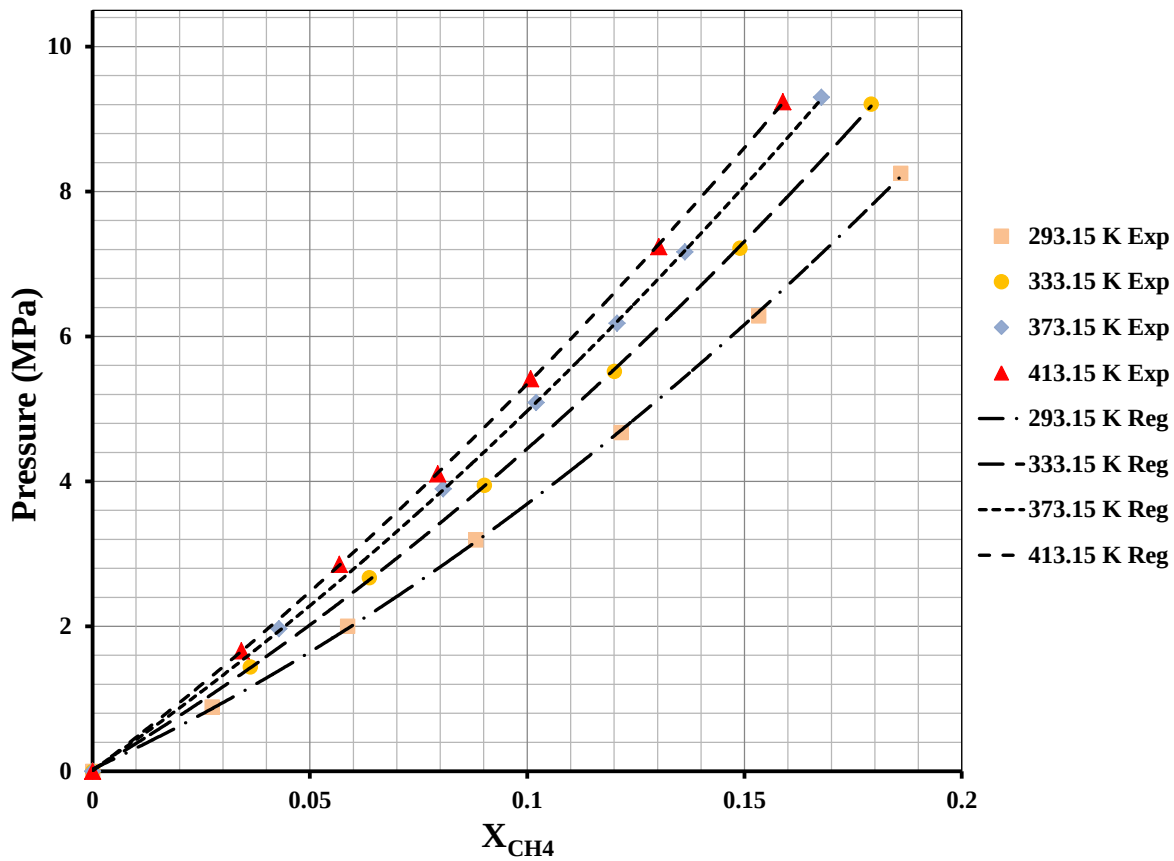

Figure 14: Comparison Between Experimental and Predicted CH_4 Mole Fractions in [hmim][Tf2N] at Different Pressures and Temperatures

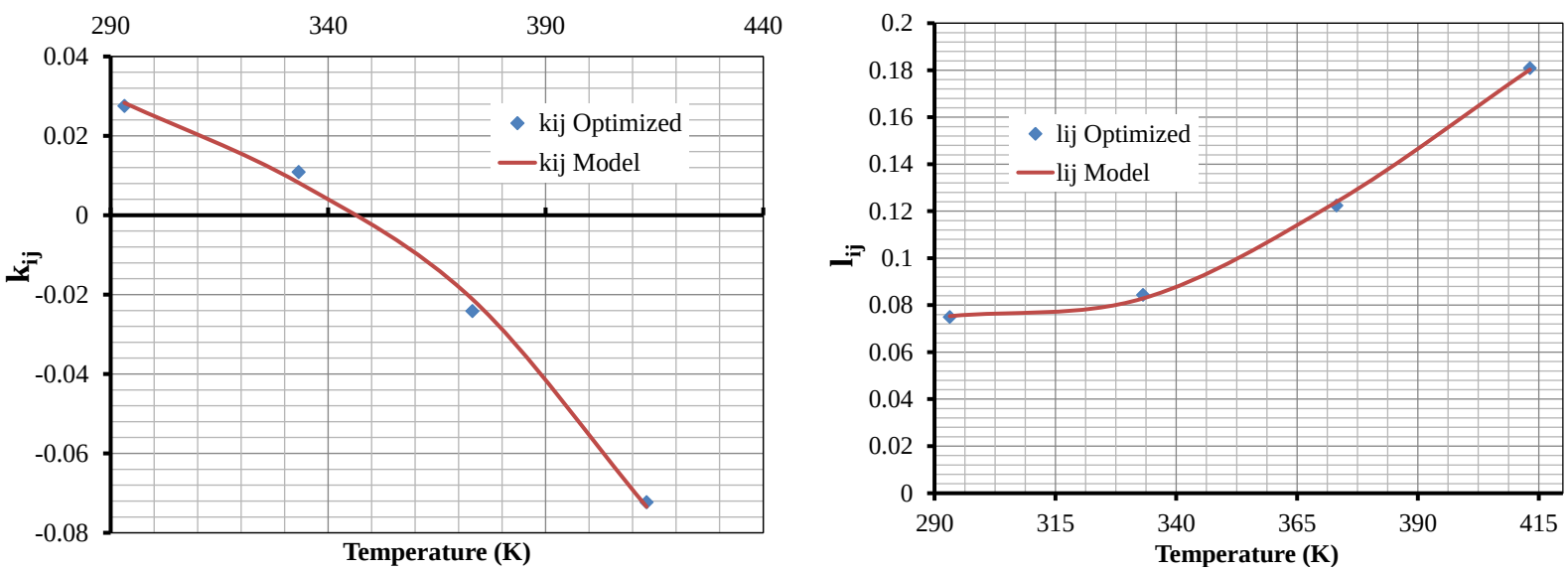

Figure 15: Optimized Binary Interaction Parameters for CH_4 in [hmim][Tf2N]

4.5. CO DATA:

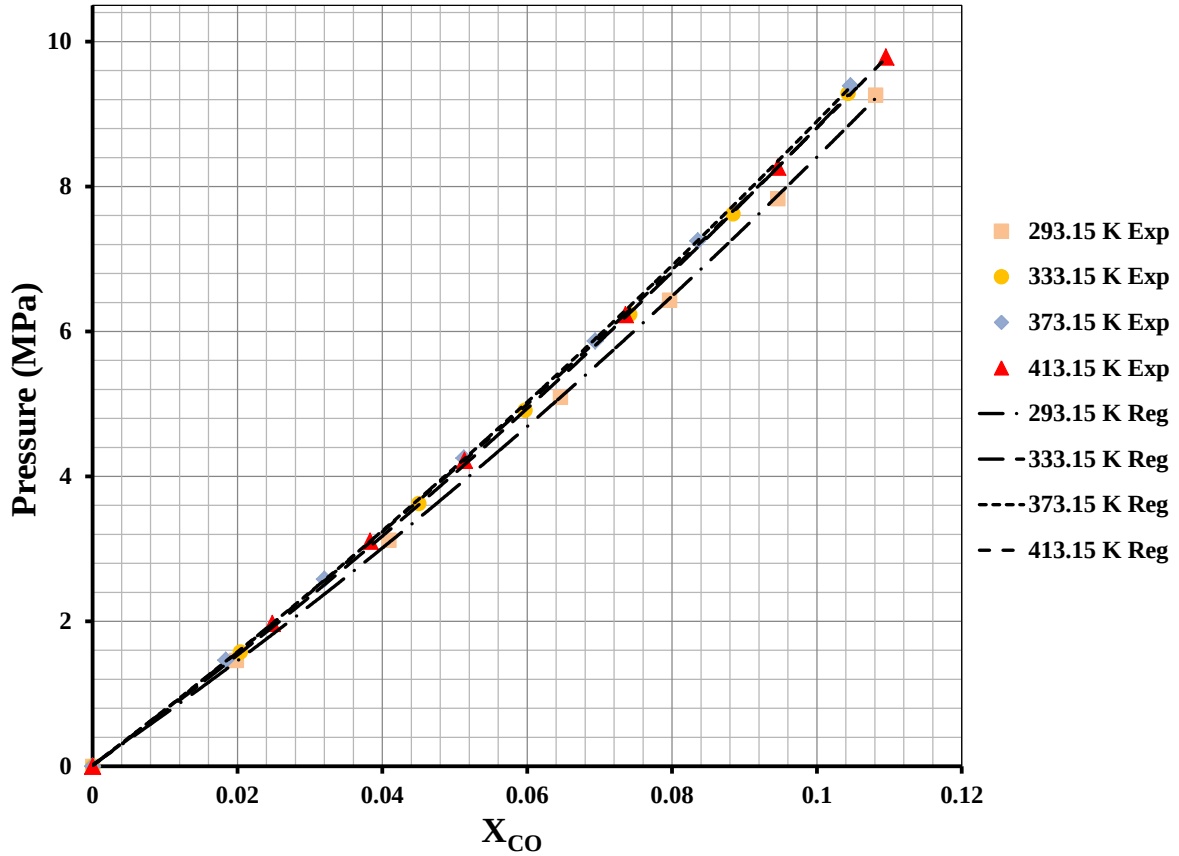

Figure 16: Comparison Between Experimental and Predicted CO Mole Fractions in [hmim][Tf2N] at Different Pressures and Temperatures

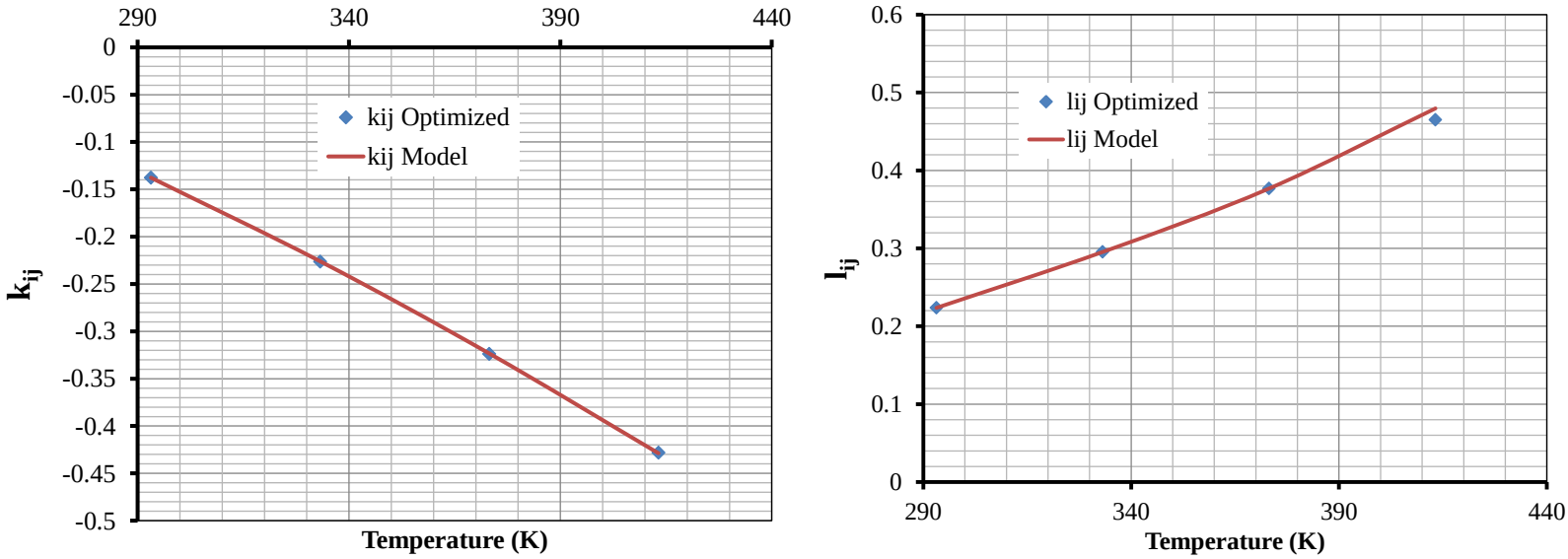

Figure 17: Optimized Binary Interaction Parameters for CO in [hmim][Tf2N]

It should be mentioned that in the absence of the experimental solubility data for CO_2 in [hmim][Tf2N] at high temperature, the Span-Wagner EOS [1] was used to calculate such data as shown in Figure 18. Details of these calculations are given in the following section.

Additionally, due to the lack of experimental data on the solubility of water in [hmim][Tf2N], P-T-X values were predicted using the Peng Robinson EOS with the binary interaction parameters set to zeros.

5. CALCULATION OF THE P-T-X DIAGRAM FOR CO2 IN [HMIM][TF2N] USING SPAN-WAGNER EOS

Kumełan et al. [34] proposed Equation (16) to predict Henry's Law constant at given pressure and temperature for CO_2 in [hmim][Tf2N] IL:

$$k_{H,CO_2}(T,P) = k^{(0)}_{H,CO_2}(T)\exp\left(\frac{V^{\infty}_{m,CO_2}P}{RT}\right) \tag{16}$$

$k^{(0)}_{H,CO_2}$ was calculated using Equation (17):

$$k^{(0)}_{H,CO_2}(T) = \exp\left(7.3141 - \frac{1838.8}{T} - 0.002809 \cdot T\right) \tag{17}$$

The partial molar volume of CO_2 at infinite dilution, V^{∞}_{m,CO_2}, was calculated from Equation (18)

$$V^{\infty}_{m,CO_2} = -162.8 + 0.1365 \cdot T \tag{18}$$

The CO_2 activity, $a_{CO_2}(T, m_{CO_2})$, in the IL was calculated using Equation (19):

$$a_{CO_2}(T, m_{CO_2}) = \frac{m_{CO_2}}{m^o}\gamma^*_{CO_2} \tag{19}$$

In this Equation, m_{CO_2} is the solubility of CO_2 in [hmim][Tf2N], expressed in $(mol)_{CO2}/(kg)_{IL}$, and m^o = 1 mol/kg.

The value of m_{CO_2} at any pressure and temperature (*P, T*) can be related to the CO_2 mole fraction (x_{CO2}) by Equation (20) as:

$$x_{CO2} = \frac{(m_{CO2})Mwt_{IL}}{1 + (m_{CO2})Mwt_{IL}} \tag{20}$$

Where $(Mwt)_{IL}$ is the molecular weight of the [hmim][Tf2N].

The CO_2 activity coefficient, $\gamma^*_{CO_2}$, was calculated from Equations (21) and (22):

$$\gamma^*_{CO_2} = exp\left(2\frac{m_{CO_2}}{m^o}\sigma^{(0)}_{CO_2,CO_2}\right) \tag{21}$$

$$\sigma^{(0)}_{CO_2,CO_2} = 0.20914 - \frac{72.12}{T} \tag{22}$$

From the above Equations, the fugacity of CO_2 in [hmim][Tf2N], $f_{CO_2}(T,P)$, was calculated from Equation (23):

$$f_{CO_2}(T,P) = k_{H,CO_2}(T,P) \cdot a_{CO_2}(T, m_{CO_2}) \tag{23}$$

The fugacity of CO_2 in the [hmim][Tf2N] IL can also be calculated from Equation (24), if the system pressure and the CO_2 fugacity coefficient are known.

$$f_{CO_2}(T,P) = P \cdot \varphi_{CO_2}(T,P) \tag{24}$$

In 1996, Span and Wagner [1] reviewed the available data on CO_2 thermodynamic properties and presented a new Equation of State (EOS) in the form of a fundamental Equation explicit in the Helmholtz Free Energy (HFE) where the function for the residual part of the HFE was fitted to selected data of the fugacity coefficient and other important CO_2 thermodynamic properties. According to Span and Wagner [1], the CO_2 fugacity coefficient can be calculated using Equations (25) through (35):

$$\varphi_{CO_2}(T,P) = exp(\phi^r + \delta\phi_\delta^r - \ln(1 + \delta\phi_\delta^r)) \tag{25}$$

$$\phi^r = \sum_{i=1}^{7} n_i \delta^{d_i} \tau^{t_i} + \sum_{i=8}^{34} n_i \delta^{d_i} \tau^{t_i} e^{-\delta^{c_i}} + \sum_{i=35}^{39} n_i \delta^{d_i} \tau^{t_i} e^{-\alpha_i(\delta-\epsilon_i)^2 - \beta_i(\tau-\gamma_i)^2} + \sum_{i=40}^{42} n_i \Delta^{b_i} \delta \Psi \tag{26}$$

$$\delta = \rho/\rho_c \tag{27}$$
$$\tau = T_c/T \tag{28}$$
$$\Delta = \theta^2 + B_i[(\delta-1)^2]^{\alpha_i} \tag{29}$$
$$\theta = (1-\tau) + A_i[(\delta-1)^2]^{1/(2\beta_i)} \tag{30}$$
$$\Psi = e^{-C_i(\delta-1)^2 - D_i(\tau-1)^2} \tag{31}$$

$$\begin{aligned}\phi_\delta^r = &\sum_{i=1}^{7} n_i d_i \delta^{d_i-1} \tau^{t_i} + \sum_{i=8}^{34} n_i e^{-\delta^{c_i}} [\delta^{d_i-1} \tau^{t_i} (d_i - c_i \delta^{c_i})] \\ &+ \sum_{i=35}^{39} n_i \delta^{d_i} \tau^{t_i} e^{-\alpha_i(\delta-\epsilon_i)^2 - \beta_i(\tau-\gamma_i)^2} \left[\frac{d_i}{8} - 2\alpha_i(\delta-\epsilon_i)\right] \\ &+ \sum_{i=40}^{42} n_i \left[\Delta^{b_i}\left(\Psi + \delta\frac{\partial\Psi}{\partial\delta} + \frac{\partial\Delta^{b_i}}{\partial\delta}\delta\Psi\right)\right]\end{aligned} \tag{32}$$

$$\frac{\partial\Psi}{\partial\delta} = -2C_i(\delta-1)\Psi \tag{33}$$

$$\frac{\partial\Delta^{b_i}}{\partial\delta} = b_i \Delta^{b_i} \left(\frac{\partial\Delta}{\partial\delta}\right) \tag{34}$$

$$\frac{\partial\Delta}{\partial\delta} = B_i(2\alpha_i)(\delta-1)^{2(\alpha_i-1)} + 2\theta A_i(1/\beta_i)(\delta-1)^{(1/\beta_i-1)} \tag{35}$$

All coefficients in the above Equations are given in Table 4. Using the above Equations, an algorithm was built where at a given pressure and temperature (P, T), Equations (23) and (24) were equated and the value of the mole fraction *X* was calculated. Accordingly, a P-T-X diagram for the CO_2 – [hmim][Tf2N] IL

was constructed. It should be emphasized that the predictions of the algorithm were compared with many available experimental data [4], [30], [35], including those measured in this study at NETL-DOE for CO_2 – [hmim][Tf2N] IL and a very good agreement was observed. Figure 18 shows such predictions and as can be seen the solubility of CO_2 in the [hmim][Tf2N] systematically decreases with increasing temperatures at constant pressure. For instance at 3 MPa, the mole fraction of CO_2 in the IL is 0.47 at 298.15 K and this value decreases to 0.12 at 510 K. It should be emphasized that the P-T-X diagram generated in this study fits the data very well.

Table 4: Coefficients in Equations (25) Through (35)

i	n_i	d_i	t_i
1	3.88568232031610E-01	1	0.00
2	2.93854759427400E+00	1	0.75
3	-5.58671885349340E+00	1	1.00
4	-7.67531995924770E-01	1	2.00
5	3.17290055804160E-01	2	0.75
6	5.48033158977670E-01	2	2.00
7	1.22794112203350E-01	3	0.75

i	n_i	d_i	t_i	c_i
8	2.16589615432200E+00	1	1.5	1
9	1.58417351097240E+00	2	1.5	1
10	-2.31327054055030E-01	4	2.5	1
11	5.81169164314360E-02	5	0.0	1
12	-5.53691372053820E-01	5	1.5	1
13	4.89466159094220E-01	5	2.0	1
14	-2.42757398435010E-02	6	0	1
15	6.24947905016780E-02	6	1	1
16	-1.21758602252460E-01	6	2	1
17	-3.70556852700860E-01	1	3	2
18	-1.67758797004260E-02	1	6	2
19	-1.19607366379870E-01	4	3	2
20	-4.56193625087780E-02	4	6	2
21	3.56127892703460E-02	4	8	2
22	-7.44277271320520E-03	7	6	2
23	-1.73957049024320E-03	8	0	2
24	-2.18101212895270E-02	2	7	3
25	2.43321665592360E-02	3	12	3
26	-3.74401334234630E-02	3	16	3
27	1.43387157568780E-01	5	22	4
28	-1.34919690832860E-01	5	24	4
29	-2.31512250534800E-02	6	16	4
30	1.23631254929010E-02	7	24	4
31	2.10583219729400E-03	8	8	4
32	-3.39585190263680E-04	10	2	4
33	5.59936517715920E-03	4	28	5
34	-3.03351180556460E-04	8	14	6

i	n_i	d_i	t_i	α_i	β_i	γ_i	ε_i
35	-2.13654886883200E+02	2	1	25	325	1.16	1
36	2.66415691492720E+04	2	0	25	300	1.19	1
37	-2.40272122045570E+04	2	1	25	300	1.19	1
38	-2.83416034239990E+02	3	3	15	275	1.25	1
39	2.12472844001790E+02	3	3	20	275	1.22	1

i	n_i	a_i	b_i	β_i	A_i	B_i	C_i	D_i
40	-6.66422765407510E-01	3.5	0.875	0.3	0.7	0.3	10	275
41	7.26086323498970E-01	3.5	0.925	0.3	0.7	0.3	10	275
42	5.50686686128420E-02	3	0.875	0.3	0.7	1	12.5	275

T_c = 34.1282 K, ρ_c = 467.6 kg/m3

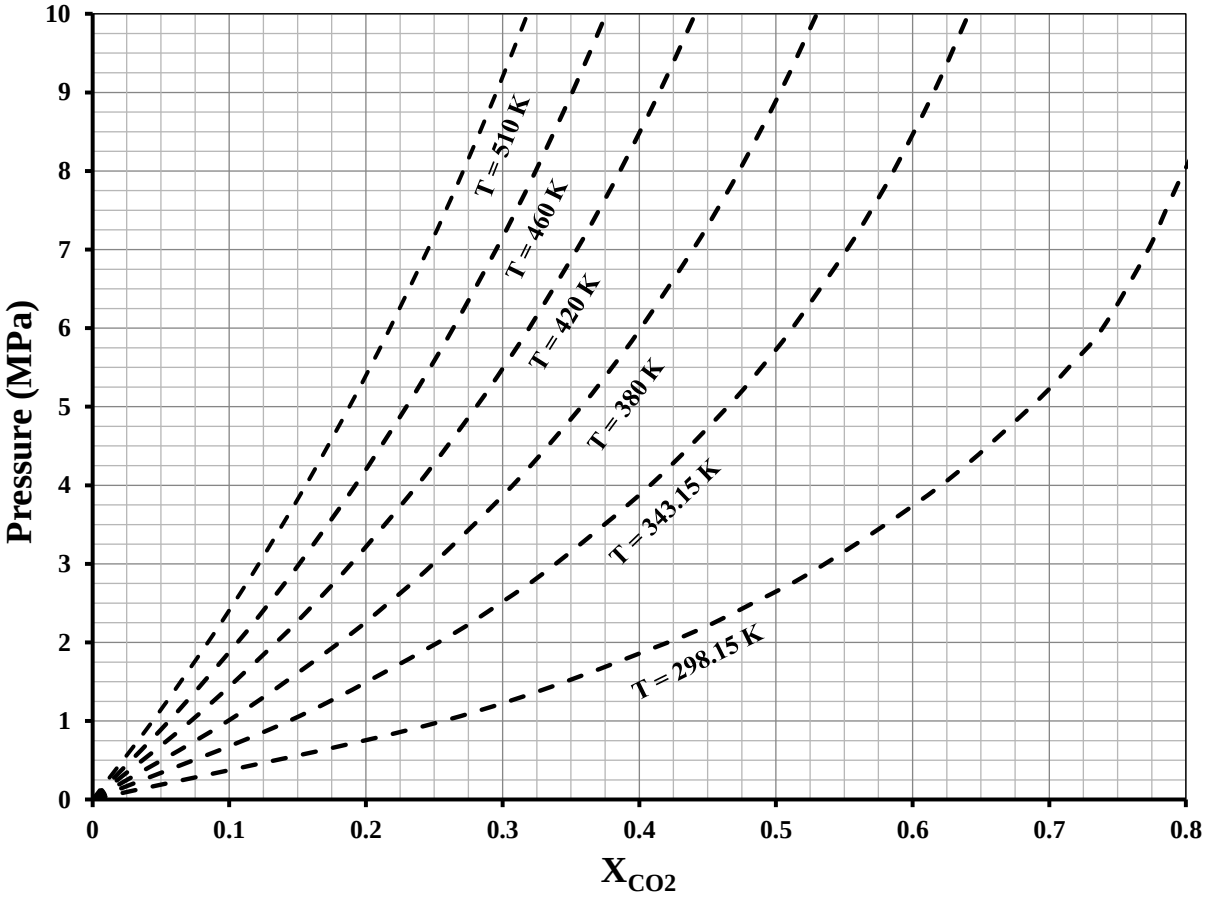

Figure 18: P-T-X Diagram for CO_2 - [hmim][Tf2N] System

6. DEVELOPMENT OF THE CO_2 CAPTURE CONCEPTUAL PROCESS USING [HMIM][TF2N]

The conceptual process is using [hmim][Tf2N] as a physical solvent to selectively capture CO_2 from a fuel gas stream generated from an E-Gas gasifier using Pittsburgh #8 coal and shifted to a pressure and temperature of 381 psia (26.27 bar) and 857 °F (731.48 K), respectively. The composition of this shifted gas, given in Table 1, is taken from "Capital and Operating Cost of Hydrogen Production from Coal Gasification", Final Report, April 2003, by Parsons [36]. The apparent molecular weight of this shifted gas stream is 19.055 kg/kmol. Shuster et al. [19] reported in the Interim Report "Systems Analysis Study on the Development of Fluorinated Solvents for Warm-Temperature/High-Pressure CO_2 Capture of Shifted Syngas" April 19, 2005, that the fuel gas stream for a 400-MWe power plant is 813,643 lb/h (102.52 kg/s) or 5.38 kmol/s.

In the Aspen Plus simulation of the conceptual process development, the pressure and temperature of the shifted gas stream was set to 30 bar and 500 K, respectively. The process consists of 4 identical adiabatic packed-bed absorbers arranged in parallel (Figure 19) to handle the total shifted gas mass flow rate of 102.52 kg/s. In order to capture CO_2 from this gas stream, 4,150 kg/s of [hmim][Tf2N] are

required. Thus, each packed-bed is to handle 25.63 kg/s (1.345 kmol/s) of the shifted gas and 1,037.5 kg/s (2,173.14 kmol/s) of the [hmim][Tf2N] solvent.

The shifted gas enters each packed-bed absorber from the bottom at 500 K and the solvent enters each absorber from the top at 298 K in a counter-current scheme. In each absorber, the [hmim][Tf2N] solvent is heated by the sensible heat of the gas to 467.8 K. In the continuous process, 0.0289 kmol/s (12.93 kg/s) of [hmim][Tf2N] was needed to make up for the solvent losses during the CO_2 capture and regeneration steps. Table 5 shows the solvent losses in the main process streams.

Table 5: Solvent loss streams

Flow rate in kmol/s	[hmim][Tf2N]
CO_2 stream	0.0008
H_2 stream	0.0000
H_2O stream	0.0281
Total amount of solvent lost	0.0289

The packed-bed absorber characteristics and packing specifications used in the Aspen Plus simulation are given in Table 6.

Table 6: Packed-bed and packing specifications

Description	Unit	Value
Packed column diameter	m	2.4
Packed bed cross section area	m^2	4.52
Number of stages	-	10
Height of each stage	m	3
Packed bed height	m	30
Packing type	-	Plastic Pall Rings
Packing dimension	m	0.025 (1”)
Packing surface area	m^2/m^3	205
Void fraction	-	0.90
Gas flow rate	kg/s	25.63
Liquid flow rate	kg/s	1037.5

The gas-solvent mass transfer in the packed-bed, was accounted for using the Billet and Schulte’s Correlations [37], which were proposed to estimate the mass transfer coefficients and the effective gas-liquid interfacial area in packed-beds with random and structured packing. The liquid-phase binary mass transfer coefficient ($K_{i,k}^{L}$) is defined in Aspen Plus as:

$$k_{i,k}^{L} = C_L \left(\frac{g\rho_L}{\mu^L} \right)^{0.167} \sqrt{\frac{D_{i,k}^{L}}{d_h}} \left(\frac{u_s^L}{a_p} \right)^{0.333} \tag{36}$$

With a default value of C_L = 0.905.

The total interfacial area for mass transfer (a^I) is defined by:

$$a^I = a_e A_t h_p \tag{37}$$

The effective area (a_e) per unit volume of the bed is related to the specific area of packing (a_P) through the following Equation:

$$\frac{a_e}{a_p} = \frac{1.5}{\sqrt{a_p d_h}} Re_L^{-0.2} We_L^{0.75} Fr_L^{-0.45} \tag{38}$$

The volumetric mass transfer coefficients ($k_L a$) for CO_2 in the solvent were calculated from the liquid-phase binary mass transfer coefficient ($K_{i,k}^L$) obtained from Aspen Plus, where (i) and (k) stand for CO_2 and the solvent, respectively, using the following Equation:

$$k_L a = k_{i,k}^L \cdot a_e = \frac{K_{i,k}^L}{\overline{\rho}_L \cdot a^I} \times a_e \tag{39}$$

Figure 19 shows that following the gas absorption in the 4 packed beds, the gas streams (IL-poor) from the top of the absorbers are combined in one stream; and the liquid streams (IL-rich) from the bottom of the 4 absorbers are also combined in one stream. The IL-rich stream is regenerated using the pressure-swing option with 3 adiabatic flash drums arranged in series at different pressures 20, 10 and 1 bar, respectively. These flash drums allow the separation of the absorbed gases from the IL into a CO_2-rich gas-stream, containing some H_2 and H_2O vapor at about 468 K, and an IL solvent-rich stream containing some CO_2, H_2 and other dissolved gaseous constituents.

The gas streams leaving the top of the 3 flash drums are cooled to 288 K to separate any water present and then are combined into one stream. This stream is compressed to 55 bar, followed by intercooling to 223 K. The system was then sent to a separator to remove the condensed water and the CO_2 stream was pumped to 153 bar to the sequestration site. The H_2 stream was also compressed to 153 bar followed by intercooling at 223 K and a separator in order to capture any remaining CO_2 present in this stream. The captured CO_2 is combined with that from the pump and sent to the sequestration site. The separated H_2 stream was then expanded to 100 bar, combined with the overhead stream from the 4 absorbers and heated to 1500 K before sending to turbines as depicted in Figure 19.

Also, the IL-rich stream from the bottom of the third flash drum at 1 bar is pumped to 30 bar and recycled back to the packed-bed absorbers where the required make-up solvent is added to it at 298 K prior entering the absorbers.

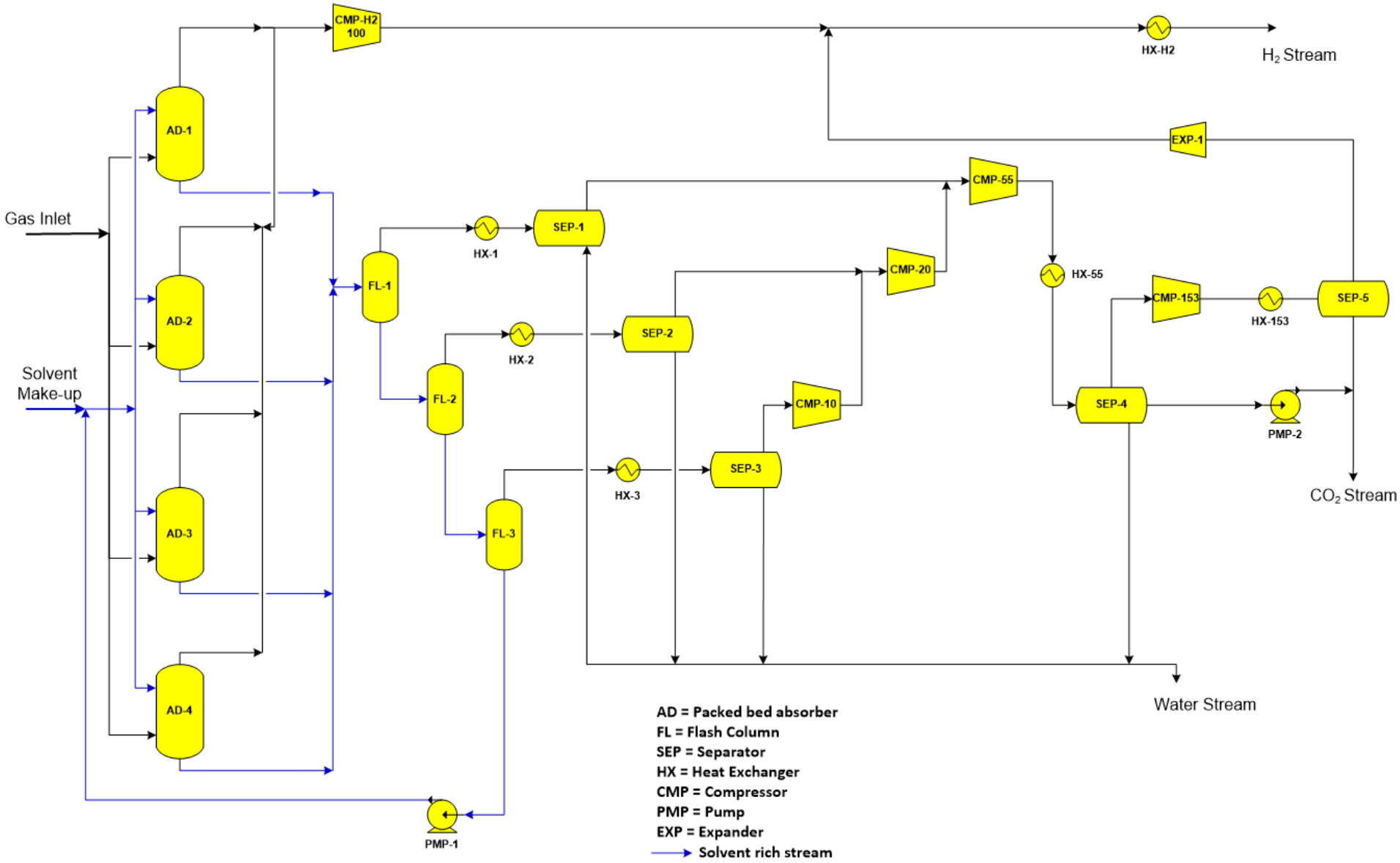

Figure 19: Schematic of the Conceptual Process for CO_2 Capture using [hmim][Tf2N]

7. SIMULATION RESULTS

The composition of the combined outlet liquid stream from the 4 packed absorbers expressed in molar flow rate and percentage of the inlet feed molar flow rate to the absorbers, is presented in Table 7. As can be seen 91.99 mol% of the CO_2, 3.5 mol% of H_2, 99.99 mol% of H_2S and 99.98 mol% of H_2O are captured using the [hmim][Tf2N] solvent, and a negligible amount of the solvent is lost at this stage of the process.

Table 7: Composition of the outlet liquid stream from the 4 packed absorbers

	[hmim][Tf2N]	
Component	Inlet mole flow rate	Percentage of the inlet stream
	kmol/hr	mol%
Ar	61.2	65.9
CH_4	40.6	87.4
H_2	249.8	3.5
N_2	39.19	61.32
CO	779.6	64.19
CO_2	4,596.23	91.99
H_2O	5,942.1	99.98
NH_3	30.99	99.99
H_2S	91.03	99.99
Solvent	40,230.66	99.99

These results show that at the absorber conditions, the [hmim][Tf2N] IL could achieve a CO_2 recovery about 92%, an H_2S recovery of 99.99%, while maintaining a low H_2 absorption of 3.5%. Nonetheless, a significant amount of CO has been absorbed in the solvent (64.19%) and therefore additional processing units were added to maximize recovery of both CO and H_2.

Based on the inlet gas stream composition, the CO_2-rich stream which is sent to the sequestration site at 153 bar and 223 K contains 95.6 mol% of CO_2, 0.334 mol% of H_2 and 90.83 mol% of H_2S; and the H_2-rich stream which is sent to turbines at 100 bar and 1500 K contains 99.5 mol% of H_2, 91.97 mol% of CO, 1.55 mol% of CO_2 and 0.01 mol% of H_2O vapor (Table 8). Likewise, based on the inlet gas stream composition, the water-stream separated from the system at 287.3 K and 1 bar contains 91.07 mol% of H_2O and 90.73 mol% of NH_3 and 1.37 mol% of H_2S; and the recycled IL-stream contains 8.74 mol% of H_2O, 0.34 mol% of CO_2, and 0.001 mol% of H_2 (Table 8).

Table 8: Composition of the outlet streams from the conceptual process based on the inlet gas composition for the [hmim][Tf2N] solvent

	Gas Inlet stream	CO_2 stream	H_2 stream	H_2O stream	[hmim][Tf2N] recycle stream
	kmol/hr	mol%	mol%	mol%	mol%
Ar	92.97	12.79	83.35	1.8	0.016
CH_4	46.48	16.99	80.57	2.17	0.262
H_2	7263	0.334	99.5	0.097	0.001
N_2	63.91	11.92	86.37	1.65	0.046
CO	1214.37	6.24	91.97	1.71	0.059
CO_2	4623.14	95.67	1.55	2.43	0.34
H_2O	5942.10	0.18	0.01	91.07	8.74
NH_3	30.99	8.24	0.001	90.73	1.02
H_2S	91.0296	90.83	0.92	1.37	7.99
T (K)	500	223	1500	287.3	467.8
P (bar)	30	153	100	1	30

The distribution of the cooling in the 3 flash drums (**HX-1**, **HX-2** and **HX-3)** was found to be different since decreasing the pressure from 30 to 1 bar in 3 steps changes the flow rates of the vapor and liquid phases exiting within the units.

Table 9 shows details of the power duty and requirements for each unit presented in Figure 19. The 4 packed absorbers and the three flash drums have no power requirements as they are operated adiabatically. The largest power consumptions are for heating and cooling of the CO_2 streams (**HX-1**, **HX-2**, **and HX-3**) after the flash drums and the intercooling (**HX-55**) during CO_2 compression, which represents -102.11 MW and -30.04 MW, respectively. Heating the H_2 streams to 1500 K before sending to the turbines (**HX-H2**) requires 66.64 MW. The power for the pump (**PMP-1**) required to recycle the IL stream back to the absorbers at 30 bar is 12.34 MW, whereas that of the pump needed to send CO_2 to sequestration sites at 153 bar is 0.626 MW.

These results show that the net power balance of the proposed conceptual process is negative (-30.81 MW), which could be employed to generate utilities or perhaps be used to heat other streams in a wider total plant integration scheme.

Table 9: Power duty of the conceptual process

Units	Description	Power
		MW
AB-1	Packed-Bed Absorbers	0.00
AB-2		0.00
AB-3		0.00
AB-4		0.00
FL-1	Flash Drums	0.00
FL-2		0.00
FLA-3		0.00
CMP-H2	Compressor to boost H_2 to 100 bar	14.6
HX-H2	Heater to heat H_2 to 1500 K	66.635
HX-1	Heat exchanger to cool CO_2 stream to 288 K	-61.1
HX-2		-6.09
HX-3		-34.92
SEP-1	Separator to separate CO_2 gas from IL after cooling to 288 K	-0.123
SEP-2		-0.001
SEP-3		-0.10
CMP-10	CO_2 compressor to 10 bar	1.22
CMP-20	CO_2 compressor to 20 bar	0.801
CMP-55	CO_2 compressor to 55 bar	6.54
HX-55	Intercooling to 223 K	-30.04
SEP-4	Separation of Liquid CO_2 from CO_2 stream containing H_2	-0.505
CMP-153	CO_2 compressor to 153 bar	1.03
HX-153	Intercooling to 223 K	-1.57
SEP-5	Separation of Liquid CO_2 from CO_2 stream containing H_2	0.00
Exp-1	Expander for H_2 stream	-0.15
PMP-1	Pump to bring the IL back to 30 bar for recycling	12.34
PMP-2	Pump to send CO_2 to sequestration sites at 153 bar	0.626
Net Power		-30.81

7.1. EFFECT OF PACKED-BED ABSORBER HEIGHT ON CO_2 CAPTURE:

Figure 20 shows the effect of the height of the packed bed on the absorption of CO_2, H_2 and CO by [hmim][Tf2N], and as can be seen increasing the maximum height beyond 30 m does not lead to any significant improvement in the absorption of these gases. Thus, the optimum height where there is a maximum CO_2 absorption and a minimum H_2 and CO absorption can in reached at 30 m. Numerical difficulties prevented the evaluation at bed heights lower than 27 m as the process simulation in Aspen Plus failed to converge.

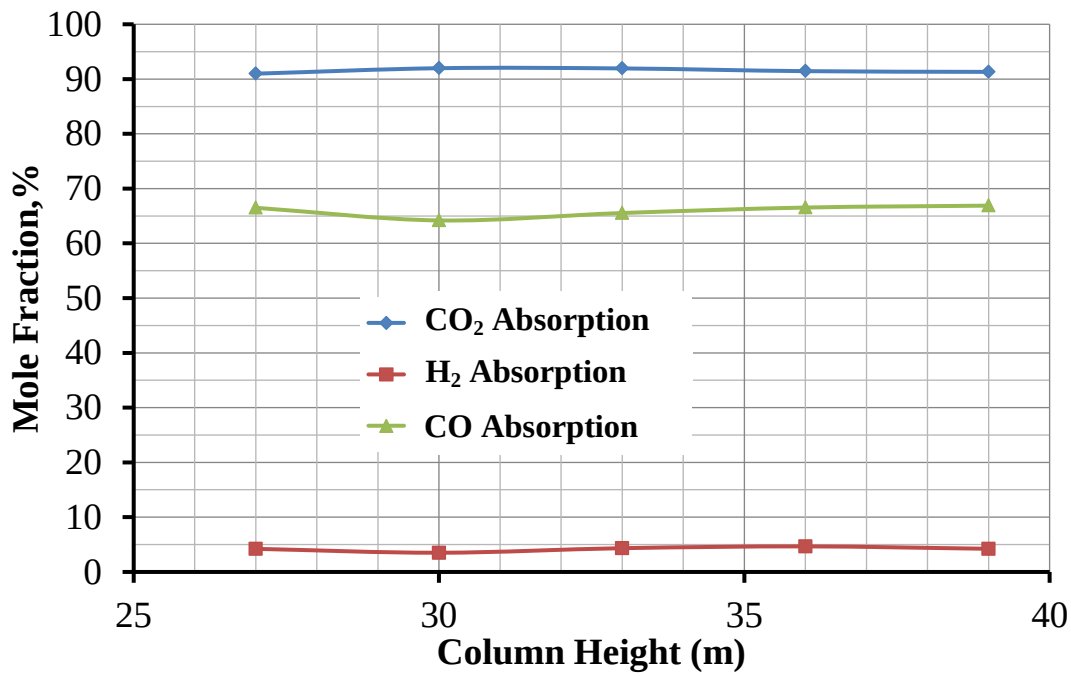

Figure 20: Effect of Packed Bed Height on CO_2, H_2 and CO Absorption

8. CONCLUSIONS

A conceptual process for CO_2 capture from a warm shifted fuel gas stream produced from Pittsburgh # 8 coal for a 400 MWe power plant using [hmim][Tf2N] IL was developed. Available experimental data in literature were used to estimate the ionic liquid physical and thermodynamic parameters. Moreover, the binary interaction parameters for the Peng Robinson Equation of State with Boston Mathias (BM) alpha function and standard mixing rules were optimized. The conceptual process was simulated using Aspen Plus v7.2 and the compositions of the process streams, CO_2 capture efficiency, and net power were calculated. The compositions of the main four process streams, CO_2-rich, H_2-rich, water, and IL-rich, were expressed as a percentage of the composition of the inlet gas stream to the absorbers.

Based on the inlet gas stream composition, the CO_2-rich stream sent to the sequestration site at 135 bar and 223 K contains 95.6 mol% of CO_2, 0.334 mol% of H_2 and 90.83 mol% of H_2S; the H_2-rich stream sent to turbines at 100 bar and 1500 K contains 99.5 mol% of H_2, 91.97 mol% of CO, 1.55 mol% of CO_2 and 0.01 mol% of H_2O vapor. Also, based on the inlet gas stream composition, the water-stream is separated from the system at 287.3 K and 1 bar and contains 91.07 mol% of H_2O and 90.73 mol% of NH_3 and 1.37 mol% of H_2S; and the recycled IL-stream to the absorbers contains 8.74 mol% of H_2O, 0.34 mol% of CO_2, and 0.001 mol% of H_2, where the IL exhibited a negligible loss of 0.31 mol%.

In addition, the conceptual process generated 30.81 MW of surplus power which could be used in numerous energy and cost saving activities throughout the plant. These results indicate that [hmim][Tf2N] IL could be used as a physical solvent for CO2 capture from warm shifted fuel gas streams.

ACKNOWLEDGMENT

As part of the National Energy Technology Laboratory's Regional University Alliance (NETL-RUA), a collaborative initiative of the NETL, this technical effort was performed under the RES contract DE-FE0004000.

DISCLAIMER

The views and opinions of authors expressed herein do not necessarily state or reflect those of the United States Government or any agency thereof.

NOMENCLATURE

a_e	Effective area per unit volume of the column	m^{-1} [=] $m^2.m^{-3}$	
a^I	Total interfacial area for mass transfer	m^2	
a_p	Specific area of packing	m^{-1} [=] $m^2.m^{-3}$	Specified on the Pack Rating | Results sheet as the Surface area in $m^2.m^{-3}$
A_t	Cross-sectional area of the column	m^2	
C_L	Mass transfer coefficient parameters for liquid, characteristic of the shape and structure of the packing	-	Specified on the Pack Rating | Rate-Based | Correlations sheet
d_h	Hydraulic diameter	m	$\frac{4\varepsilon}{a_p}$
$D_{i,k}^L$	Diffusivity of the liquid	$m^2.s^{-1}$	
Fr_L	Froude number for the liquid	-	$\frac{a_p (u_S^L)^2}{g}$
g	Gravitational constant	$m.s^{-2}$	
h_p	Height of the packed section	m	This is the total height of the column divided by the number of stages or directly given by the packed height per stage
$k_L a$	Liquid side volumetric mass transfer coefficient	s^{-1}	
$k_{i,k}^L$	Binary mass transfer coefficient for the liquid	$m.s^{-1}$	
$K_{i,k}^L$	Liquid-phase binary overall mass transfer coefficient	$kmol.s^{-1}$	$k_{i,k}^L \overline{\rho}_L a^I$
L	Molar flow rate of liquid	$kmol.s^{-1}$	
Mwt	Molecular weight	$kg.kmol^{-1}$	
P_c	Critical pressure	bar	
P^s	Vapor pressure	bar	
Re_L	Reynolds number for the liquid	-	$\frac{\rho_L u_S^L}{a_p \mu^L}$
T_b	Boiling point temperature	K	
T_c	Critical temperature	K	

u_s^L	Superficial velocity for the liquid	m.s^{-1}	$\frac{L}{\overline{\rho}_L A_t}$
V_c	Critical volume	m^3.kmol^{-1}	
We_L	Weber number for the liquid	-	$\frac{\rho_L \left(u_S^L\right)^2}{a_p \sigma}$
x^*	Solubility, mole of gas per total number of mole	-	
Z_c	Critical compressibility	-	
ΔT_b	Contribution to the normal boiling temperature in the Modified Lydersen-Joback-Reid method	K	
ΔP_c	Contribution to the critical pressure in the Modified Lydersen-Joback-Reid method	bar	
ΔT_c	Contribution to the critical temperature in the Modified Lydersen-Joback-Reid method	K	
ΔV_c	Contribution to the critical volume in the Modified Lydersen-Joback-Reid method	cm^3.mol^{-1}	
δ_{ij}	Peng-Robinson binary interaction parameter	-	
ε	Void fraction of the packing	-	
μ_L	Liquid viscosity	Pa.s	
ρ_L	Liquid density	kg.m^{-3}	
$\overline{\rho}_L$	Molar density of liquid	kmol.m^{-3}	
σ_L	Liquid surface tension	N.m^{-1}	
ω	Acentric factor	-	

REFERENCES:

[1] R. Span and W. Wagner, "A New Equation of State for Carbon Dioxide Covering the Fluid Region from the Triple-Point Temperature to 1100 K at Pressures up to 800 MPa," *Journal of Physical and Chemical Reference Data*, vol. 25, no. 6, p. 1509, 1996.

[2] K. N. Marsh, J. F. Brennecke, R. D. Chirico, M. Frenkel, A. Heintz, J. W. Magee, C. J. Peters, L. P. N. Rebelo, and K. R. Seddon, "Thermodynamic and thermophysical properties of the reference ionic liquid: 1-Hexyl-3-methylimidazolium bis[(trifluoromethyl)sulfonyl]amide (including mixtures). Part 1. Experimental methods and results (IUPAC Technical Report)," *Pure and Applied Chemistry*, vol. 81, no. 5, pp. 781–790, 2009.

[3] J. a. Widegren and J. W. Magee, "Density, Viscosity, Speed of Sound, and Electrolytic Conductivity for the Ionic Liquid 1-Hexyl-3-methylimidazolium Bis(trifluoromethylsulfonyl)imide and Its Mixtures with Water †," *Journal of Chemical & Engineering Data*, vol. 52, no. 6, pp. 2331–2338, Nov. 2007.

[4] M. B. Shiflett and a Yokozeki, "Solubility of CO2 in room temperature ionic liquid [hmim][Tf2N].," *The journal of physical chemistry. B*, vol. 111, no. 8, pp. 2070–4, Mar. 2007.

[5] J. Kumełan, A. P.-S. Kamps, D. Tuma, and G. Maurer, "Solubility of H2 in the Ionic Liquid [hmim][Tf2N]," *Journal of Chemical & Engineering Data*, vol. 51, no. 4, pp. 1364–1367, 2006.

[6] J. L. Anderson, J. K. Dixon, E. J. Maginn, and J. F. Brennecke, "Measurement of SO2 solubility in ionic liquids.," *The journal of physical chemistry. B*, vol. 110, no. 31, pp. 15059–62, Aug. 2006.

[7] J. Kumełan, Á. P.-S. Kamps, D. Tuma, and G. Maurer, "Solubility of the Single Gases Methane and Xenon in the Ionic Liquid [hmim][Tf2N]," *Industrial & Engineering Chemistry Research*, vol. 46, no. 24, pp. 8236–8240, 2007.

[8] J. Kumełan, A. P.-S. Kamps, D. Tuma, and G. Maurer, "Solubility of the Single Gases Carbon Monoxide and Oxygen in the Ionic Liquid [hmim][Tf2N]," *Journal of Chemical &Engineering Data*, vol. 54, no. 3, pp. 966–971, 2009.

[9] S. Raeissi, L. J. Florusse, and C. J. Peters, "Hydrogen Solubilities in the IUPAC Ionic Liquid 1-Hexyl-3-methylimidazolium Bis(Trifluoromethylsulfonyl)Imide," *Journal of Chemical & Engineering Data*, vol. 56, no. 4, pp. 1105–1107, Apr. 2011.

[10] L. Florusse, S. Raeissi, and C. Peters, "An IUPAC Task Group Study: The Solubility of Carbon Monoxide in at High Pressures," *Journal of Chemical & …*, pp. 4797–4799, 2011.

[11] J. Anderson, "Solubility of CO2, CH4, C2H6, C2H4, O2, and N2 in 1-Hexyl-3-methylpyridinium Bis (trifluoromethylsulfonyl) imide: Comparison to Other Ionic Liquids," *Accounts of chemical …*, vol. 40, no. 11, pp. 1208–1216, 2007.

[12] E. J. Maginn, "Evaluation of Ionic Liquids in Post-Combustion CO2 Capture," in *Seventh Annual Conference on Carbon Capture and Sequestration*, 2008.

[13] M. J. Muldoon, S. N. V. K. Aki, J. L. Anderson, J. K. Dixon, and J. F. Brennecke, “Improving carbon dioxide solubility in ionic liquids.,” *The journal of physical chemistry. B*, vol. 111, no. 30, pp. 9001–9, Aug. 2007.

[14] M. G. Freire, C. M. S. S. Neves, K. Shimizu, C. E. S. Bernardes, I. M. Marrucho, J. a P. Coutinho, J. N. Canongia Lopes, and L. P. N. Rebelo, “Mutual solubility of water and structural/positional isomers of N-alkylpyridinium-based ionic liquids.,” *The journal of physical chemistry. B*, vol. 114, no. 48, pp. 15925–34, Dec. 2010.

[15] W. Shi and E. J. Maginn, “Atomistic simulation of the absorption of carbon dioxide and water in the ionic liquid 1-n-Hexyl-3-methylimidazolium Bis(trifluoromethylsulfonyl)imide ([hmim][Tf2N].,” *The Journal of Physical Chemistry. B*, vol. 112, no. 7, pp. 2045–55, Feb. 2008.

[16] W. Shi, D. Sorescu, D. Luebke, M. J. Keller, and S. Wickramanayake, “Molecular simulations and experimental studies of solubility and diffusivity for pure and mixed gases of H2, CO2, and Ar absorbed in the ionic liquid 1-n-hexyl-3-methylimidazolium bis(trifluoromethylsulfonyl)amide ([hmim][TF2N]),” *The Journal of Physical Chemistry. B*, vol. 114, no. 19, pp. 6531–6541, 2010.

[17] A. Finotello and J. Bara, “Room-temperature ionic liquids: temperature dependence of gas solubility selectivity,” *Industrial & Engineering Chemistry Research*, vol. 47, no. 10, pp. 3453–3459, May 2008.

[18] M. Gomes, “thermodynamics of solvation of carbon dioxide, ethane, and hydrogen in 1-hexyl-3-methylimidazolium bis (trifluoromethylsulfonyl) amide between temperatures of 283,” *Journal of Chemical & Engineering Data*, pp. 472–475, 2007.

[19] E. Shuster and H. McIlvried, “Systems Analysis Study on the Development of Fluorinated Solvents for Warm-Temperature/High-Pressure CO2 Capture of Shifted Syngas - Interim Report Findings,” Pittsburgh, PA, 2005.

[20] H. Tokuda, K. Hayamizu, K. Ishii, M. A. B. H. Susan, and M. Watanabe, “Physicochemical properties and structures of room temperature ionic liquids. 2. Variation of alkyl chain length in imidazolium cation.,” *The journal of physical chemistry. B*, vol. 109, no. 13, pp. 6103–10, Apr. 2005.

[21] P. N. R. Joanna Łachwa, Pedro Morgado, Jose ´ N. Canongia Lopes, and Luı Jose, M. S. S. Esperanc¸a, Henrique J. R. Guedes, “Fluid-Phase Behavior of {1-Hexyl-3-methylimidazolium Bis(trifluoromethylsulfonyl) Imide, [C6mim][NTf2], + C2-C8 n-Alcohol} Mixtures: Liquid-Liquid Equilibrium and Excess Volumes,” *Journal of Chemical & Engineering Data*, vol. 51, pp. 2215–2221, 2006.

[22] A. Muhammad, M. I. Abdul Mutalib, C. D. Wilfred, T. Murugesan, and A. Shafeeq, “Thermophysical properties of 1-hexyl-3-methyl imidazolium based ionic liquids with tetrafluoroborate, hexafluorophosphate and bis(trifluoromethylsulfonyl)imide anions,” *The Journal of Chemical Thermodynamics*, vol. 40, no. 9, pp. 1433–1438, Sep. 2008.

[23] A. Ahosseini and A. M. Scurto, “Viscosity of Imidazolium-Based Ionic Liquids at Elevated Pressures: Cation and Anion Effects,” *International Journal of Thermophysics*, vol. 29, no. 4, pp. 1222–1243, Aug. 2008.

[24] P. J. Carvalho, M. G. Freire, I. M. Marrucho, and J. Queimada, “Surface Tensions for the 1-Alkyl-3-methylimidazolium Bis(trifluoromethylsulfonyl)imide Ionic Liquids,” *Journal of Chemical & Engineering Data*, vol. 53, no. 6, pp. 1346–1350, 2008.

[25] P. Kilaru, G. A. Baker, and P. Scovazzo, “Density and Surface Tension Measurements of Imidazolium- , Quaternary Phosphonium- , and Ammonium-Based Room-Temperature Ionic Liquids : Data and Correlations,” no. 14, pp. 2306–2314, 2007.

[26] A. Ahosseini, B. Sensenich, L. R. Weatherley, and A. M. Scurto, “Phase Equilibrium, Volumetric, and Interfacial Properties of the Ionic Liquid, 1-Hexyl-3-methylimidazolium Bis(trifluoromethylsulfonyl)amide and 1-Octene,” *Journal of Chemical & Engineering Data*, vol. 55, no. 4, pp. 1611–1617, Apr. 2010.

[27] J. Klomfar, M. SouÄ?ková, and J. Pátek, “Surface tension measurements with validated accuracy for four 1-alkyl-3-methylimidazolium based ionic liquids,” *The Journal of Chemical Thermodynamics*, pp. 323–329, 2010.

[28] D. H. Zaitsau, G. J. Kabo, A. a Strechan, Y. U. Paulechka, A. Tschersich, S. P. Verevkin, and A. Heintz, “Experimental vapor pressures of 1-alkyl-3-methylimidazolium bis(trifluoromethylsulfonyl)imides and a correlation scheme for estimation of vaporization enthalpies of ionic liquids.,” *The journal of physical chemistry. A*, vol. 110, no. 22, pp. 7303–6, Jun. 2006.

[29] Y. Shimizu, Y. Ohte, Y. Yamamura, K. Saito, and T. Atake, “Low-temperature heat capacity of room-temperature ionic liquid, 1-hexyl-3-methylimidazolium bis(trifluoromethylsulfonyl)imide.,” *The journal of physical chemistry. B*, vol. 110, no. 28, pp. 13970–5, Jul. 2006.

[30] W. Ren, B. Sensenich, and A. M. Scurto, “High-pressure phase equilibria of {carbon dioxide (CO2)+n-alkyl-imidazolium bis(trifluoromethylsulfonyl)amide} ionic liquids,” *The Journal of Chemical Thermodynamics*, vol. 42, no. 3, pp. 305–311, Mar. 2010.

[31] J. O. Valderrama and R. E. Rojas, “Critical Properties of Ionic Liquids. Revisited,” *Industrial & Engineering Chemistry Research*, vol. 48, no. 14, pp. 6890–6900, 2009.

[32] P. M. Mathias, H. C. Klotz, and J. M. Prausnitz, “Equation-of-State mixing rules for multicomponent mixtures: the problem of invariance,” *Fluid Phase Equilibria*, vol. 67, pp. 31–44, Nov. 1991.

[33] O. Pfohl, S. Petkov, and G. Brunner, “PE 2000 – A Powerful Tool to Correlate Phase Equilibria,” *Herbert Utz Verlag, München*, 2000.

[34] J. Kumełan, D. Tuma, and G. Maurer, “Partial molar volumes of selected gases in some ionic liquids,” *Fluid Phase Equilibria*, vol. 275, no. 2, pp. 132–144, Jan. 2009.

[35] J. Kumełan, Á. Pérez-Salado Kamps, D. Tuma, and G. Maurer, “Solubility of CO2 in the ionic liquid [hmim][Tf2N],” *The Journal of Chemical Thermodynamics*, vol. 38, no. 11, pp. 1396–1401, Nov. 2006.

[36] Parsons, “Capital and Operating Cost of Hydrogen Production from Coal Gasification,” Pittsburgh, PA, 2003.

[37] R. Billet and M. Schultes, “Predicting mass transfer in packed columns,” *Chemical Engineering and Technology*, vol. 16, no. 1, pp. 1–9, 1993.